

THESIS FOR THE DEGREE OF DOCTOR OF PHILOSOPHY

Influence of thermal loading on mechanical properties of railway
wheel steels

Krste Cvetkovski

Department of Materials and Manufacturing Technology
CHALMERS UNIVERSITY OF TECHNOLOGY
Gothenburg, Sweden 2012

INFLUENCE OF THERMAL LOADING ON MECHANICAL PROPERTIES OF RAILWAY WHEEL STEELS

KRSTE CVETKOVSKI

© Krste Cvetkovski, 2012

ISBN 978-91-7385-750-5

Doktorsavhandlingar vid Chalmers tekniska högskola

Ny serie nr 3431

ISSN 0346-718X

Department of Materials and Manufacturing Technology

CHALMERS UNIVERSITY OF TECHNOLOGY

SE-412 96 Göteborg, Sweden

Telephone +46 (0)31 772 10 00

Printed and bound by Chalmers Reproservice

Göteborg Sweden 2012

Influence of thermal loading on mechanical properties of railway wheel steels

Krste Cvetkovski

Department of Materials and Manufacturing Technology

Chalmers University of Technology

Abstract

Material integrity and properties of wheels are critical in railway traffic, as wheels fulfil the important function of transferring load and traction from the vehicle to the rail track. Steels with a pearlitic microstructure are commonly used for wheels due to their high strength, low cost and good wear properties. However, the pearlitic microstructure and behaviour can be altered by thermal and mechanical load being present in the contact between wheel and rail. As very high power is available, a few milliseconds of time where the slip between wheel and rail becomes large can cause small material volumes in the contact to be heated several hundred degrees Celsius.

The present work was initiated with the main purpose to investigate the effects of rapid thermal heating and cooling on wheel material. Cyclic and monotonic mechanical testing was performed to study the effects of thermal softening on virgin wheel material and on used wheels taken out from service. Furthermore, material in both pearlitic and martensitic state was investigated during rapid heating and cooling cycles by methods as laser and resistive heating for different loading conditions.

It was shown that alloying composition of different wheel steels could decrease sensitivity to thermal loads, while plastic deformation had the opposite effect when the material was subjected to long time thermal loading. For the typically very short heating times present in the wheel rail interface no significant permanent effects on mechanical properties were measured for pearlitic material. However, for martensitic material, substantial permanent hardness decrease progressed within fractions of a second at elevated temperature. This rapid tempering behaviour was observed to progress even faster in the presence of an external load. Moreover, the inherent different behaviours of pearlite and martensite can result in different residual stress fields for the case of local heating on the tread surface, affected by heating rate, peak temperature and duration.

Some additional effects of frictional heating and the influence of wear debris within cracks for rolling contact fatigue cracks were also investigated by use of image and chemical analysis.

Keywords: Railway wheel steels, heat treatment, rapid heating, martensite tempering, shear deformation, low cycle fatigue, residual stress, rolling contact fatigue, contact creep.

Preface

The research presented in this thesis was carried out at the Department of Material and Manufacturing Technology, Chalmers University of Technology, during the time period October 2007 – October 2012. This thesis is based on the work contained in the following papers, referred to by Roman numerals in the text:

I - Monotonic and cyclic deformation of a high silicon pearlitic wheel steel

K. Cvetkovski, J. Ahlström, B. Karlsson

Wear, 2011, Volume 271, Issues 1–2, pp. 382-387

II - Thermal degradation of pearlitic steels: influence on mechanical properties including fatigue behaviour

K. Cvetkovski, J. Ahlström, B. Karlsson

Materials Science and Technology, 2011, Volume 27, Issue 3, pp. 648-654

III - Influence of short heat pulses on properties of martensite in medium carbon steels

K. Cvetkovski, J. Ahlström, B. Karlsson

Submitted to Materials Science and Engineering A

IV - Rapid thermomechanical tempering of iron-carbon martensite

K. Cvetkovski, J. Ahlström, C. Persson

Manuscript

V - Characterisation of plastic deformation and thermal softening of the surface layer of railway passenger wheel treads

K. Cvetkovski, J. Ahlström

Submitted to Wear

VI - Analysis of wear debris in rolling contact fatigue cracks of pearlitic railway wheels

K. Cvetkovski, J. Ahlström, M. Norell, C. Persson

Submitted to Wear

Contribution to papers

In papers I, II, IV, V and VI experimental work and processing of the data were carried out by myself. An exception is the AES, which was made with help by Dr. Mats Norell. A general work flow was followed in writing of these papers, where I wrote a first draft, whereby comments and input from co-authors were incorporated into a final version of the paper.

In paper III, I performed the analysis of the experimental data and the dilatometer trials. Laser experiments were performed by Materials Center Leoben, Austria. The numerical modelling was made by my supervisor Docent Johan Ahlström. Accordingly, the paper was written in close cooperation with the co-authors.

CONTENTS

1	Introduction.....	1
1.1	Motivation.....	1
1.2	Layout of thesis.....	1
2	Background.....	3
2.1	Wheel damage mechanisms.....	3
2.1.1	Thermal damage.....	3
2.1.2	Fatigue damage.....	5
2.2	Materials for railway wheels.....	9
2.2.1	Strengthening mechanisms of pearlite.....	9
2.2.2	Influence of alloying elements.....	10
2.3	Microstructural degeneration.....	11
2.3.1	Recovery and recrystallization.....	12
2.3.2	Spherodisation of cementite lamellas.....	13
2.3.3	Martensite formation and tempering.....	15
3	Experimental techniques: details and theory.....	17
3.1	Microstructure evaluation.....	17
3.2	Mechanical testing.....	18
3.3	Residual stress measurement.....	18
3.4	Dilatometry.....	19
3.5	Differential scanning analysis.....	19
3.6	Auger electron spectroscopy.....	20
3.7	Heat treatment.....	21
3.8	Temperature measurement.....	21
3.9	Materials.....	23
3.10	Material extraction.....	25
4	Summary of results.....	29
4.1	Influence of alloying content on stress-strain behaviour.....	29
4.2	Influence of work hardening on annealing softening.....	31
4.3	Morphology of pearlite in the tread surface.....	31
4.4	Rapid tempering of martensite.....	33
4.5	Wear residuals within developed rolling contact fatigue cracks.....	35
4.6	Concluding remarks and contribution to the field.....	36
5	Suggestions for further work.....	39
	Acknowledgements.....	41
	References.....	43

1 Introduction

This chapter contains a brief introduction to the investigated technical problem of rapid thermal heating processes of steels used for railway wheels and motivation to the present project. Also included is an overview of the outline of the current thesis and appended papers.

1.1 Motivation

The material and structural properties of wheels are of great importance in railway traffic, since they are the only path to transfer loads and traction from the vehicle to the rail track. Historically medium to high carbon steels have been used, over time developed to accommodate the heavy haul traffic and faster running passenger trains. With an expanding European market and large investment in the railway sector, train manufacturers and operators are aiming for increased train speeds and loads with retained safety and wheel maintenance costs. Thermal damage on wheels and rail is problematic, as it can lead to crack initiation, increased wear rates and deterioration of profiles [1]. With the introduction of wheel slip protection (WSP) systems in the recent years that control available traction, thermal damage should be diminished. However, due to different vehicles and varying conditions for the many wheel sets on each train, track irregularities etc. make such a system complex. As very high power is available, for even a few milliseconds of time where the slip between wheel and rail becomes large, small material volumes in the contact can be heated several hundred degrees. It seems that perfect control has not been attained yet on every fleet as thermal damage still can be observed in railway wheels.

The present project was initiated with the main purpose to investigate the effects of rapid thermal heating and cooling cycles on railway wheel steels mainly below the austenitisation temperature (A_1). The effects of microstructure, mechanical properties and associated stresses have been studied. The problem has been examined by performing laboratory experiments, and analysis of wheels taken out of service. Results have been used to broaden the understanding of annealing and tempering processes of pearlite and martensite, and for the prediction of mechanical properties and residual stresses.

1.2 Layout of thesis

The thesis consists of an introductory part to which six papers produced during the project are appended. The introduction is mainly focused on providing a background to the work in a broader perspective related to the railway field, and does not have a strong emphasis on results obtained during the thesis work. A description of the experimental work follows together with the theoretical background of the methods

used, covered to a deeper extent than in appended papers. The last chapters are summary of results and conclusions from the papers and additional work, and suggestions for further work.

Papers I and II describes mechanical and microstructural properties of virgin wheel steels material. Chemical composition, microstructure and influence of annealing on fatigue life were main topics, with focus on increased content of silicon and manganese, assumed to improve mechanical properties of wheel steels.

Paper III was focused on evaluation of plastic deformation in the tread surface of railway wheels. Plastic shear deformation was evaluated for different position and directions in the tread.

Papers IV and V deals with the process of rapid heating and cooling, by use of experimental methods as laser, resistive and furnace heating. The purpose has been to study the phenomena of annealing and tempering on pearlite and martensitic material and evaluate residual stress states as results of thermal cycling.

Paper VI is based on a wheel failure case concerning surface and sub-surface rolling contact fatigue. Possibility of frictional heating between crack faces being present within cracks and residual material observed within cracks were studied. Characterisation of chemical and mechanical properties was performed and a theory regarding the creation of the material observed within cracks was proposed.

2 Background

Static axle loads within the European rail network are typically between 15 to 25 tons and on some networks even higher loads are allowed. This load is acting within a contact zone of a few square centimetres between the wheel and rail. In addition to dynamic loads, surface irregularities and tractive forces can increase the contact forces to even higher levels. Large deformation of material in the contact surfaces of both wheel and rail are therefore unavoidable, but nevertheless have to be controlled and accounted for. To uphold an efficient and safe railroad traffic, regular maintenance is therefore necessary in addition to component design and material selection [2].

Wheel damage is typically localized at the tread and flange (Fig. 2.1). Wear, fatigue, plastic deformation and thermal input are a few of the mechanisms that may be present [3, 4]. Often several types coexist and depending on the operational conditions of the vehicle may accelerate each other. This chapter deals with an overview of some common damage mechanisms for railway wheels, material response and theory of fatigue loading, annealing softening and metallurgical aspects of studied materials.

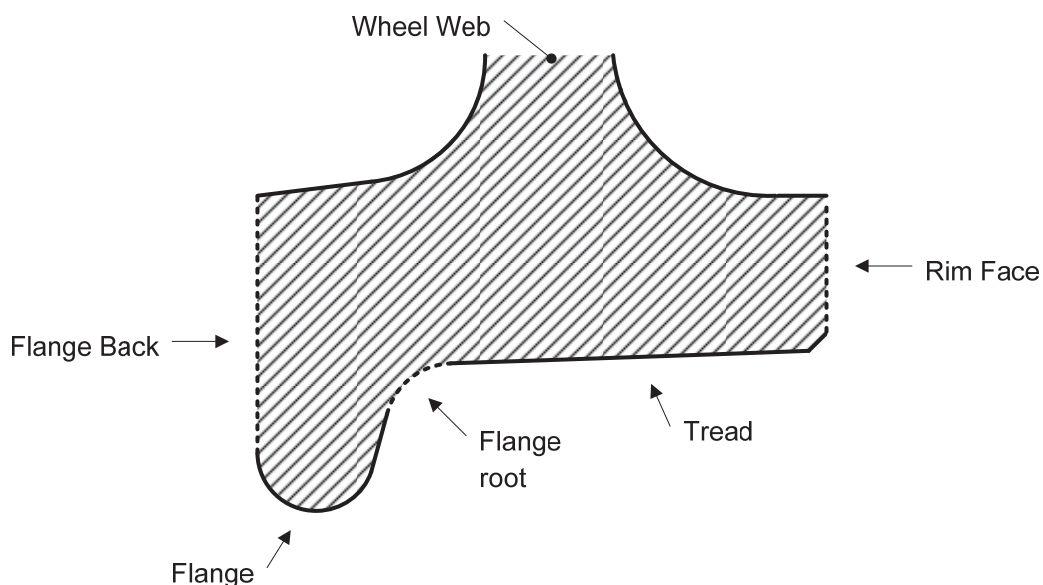


Fig. 2.1: Wheel tread cross section with associated nomenclature.

2.1 Wheel damage mechanisms

2.1.1 Thermal damage

Thermal input in a wheel with disc brakes typically arises from tractive forces, curve taking, wheel lockup, hunting oscillation etc. If these effects are large, extensive slip, i.e. creep, between wheel and rail may take place and heat can be generated due to friction and plastic deformation [5]. For a powered wheel small amounts of slip can be assumed

to be present even for normal running conditions. The contact zone can be divided in two main zones; a stick zone in the leading edge and a slip zone at the trailing edge [6-8]. It has been established that the highest temperatures are in the slip zone, as function of available adhesion, tractive force and forward speed [5]. Temperature increase in the contact zone has been predicted from few degrees for a trailing wheel, up to 200°C for a powered wheel with 2% creep in the contact [6] and 900°C for rail at a creep of 9% [8]. For low creep forces in the contact zone, primarily thermal stresses may be expected while mechanical properties and tribology behaviours remain unaffected [7]. Hence, it is apparent that control of available traction is important, if the contact temperature rises very high, the material may even undergo phase transformations, but damage can also be induced by lower temperatures of a few hundred degrees Celsius. Some different damage mechanics are here discussed:

Spalling is a type of damage caused by temperature increase in the wheel rim well above the austenitisation temperature, generally connected to wheel flats [9]. A full lock of the wheelset while the vehicle is still moving at high speed generation large amount of heat by the frictional forces in the contact patch, resulting in material transformation to austenite if the temperature reaches above the austenitisation temperature. After the slide has ceased, and the wheelset starts to rotate again, rapid cooling of the heated material volume may result in martensite formation, within a thin layer of the tread surface. In addition to the drastically changed material properties, also volume changes associated with the transformation can lead to residual compressive and tensile stresses. Martensite can also form due to very short time slip phenomena, as example when the wheel is passing insulation joints, or due to instabilities in the WSP system. For these cases the heat affected area can be very small and so also the possibly formed martensite layers, making them difficult to identify. Continuous mechanical loading within the affected area may cause crack propagation in the boundary between the martensite and surrounding material or even within, and in severe cases results in complete detachment of material in the tread, i.e. spalling. Other high temperature thermal damage types associated with immense heat generation, but perhaps more typical for tread braked wheels, are thermal cracking and crazing, which are visible as transversal cracks or micro crack patterns in the rim and tread surface [4]. Improved alloying, cleanliness of materials [10] and introduction of WSP with progress from tread to disc brakes have efficiently reduced, but perhaps not completely stopped the occurrence of high temperature related damage on passenger trains wheels. These damage types are still recurring on freight trains due to simpler tread braking systems and higher axle loads.

When temperatures are below the γ - α transformation line (A_1) the actual wheel damage may not always come directly but gradually with time due to cumulative thermal loading. For a virgin pearlitic wheel steel the permanent mechanical effects, as for example hardness, are limited after annealing below 500°C [11]. However, while the material is at elevated temperatures, mechanical properties as tensile strength, ductility, impact toughness and wear will all be altered [3, 12], making the wheel prone to

mechanical damage. The combined process of heat and deformation also may contribute to a strong alignment of the microstructure in the tread surface, giving anisotropic mechanical properties [13, 14]. Exposure of material that has work hardened to elevated temperatures for prolonged time may cause pronounced softening, due to processes as recovery or recrystallization. Thermal loading may also induce thermal stresses, giving plastic deformation and local residual stress gradients that can influence crack growth [15].

Hence, thermal damage mechanisms can progress for both low and high temperature thermal loading, in the current project the main focus has been on temperatures below A_1 .

2.1.2 Fatigue damage

2.1.2.1 Fatigue mechanisms in railway wheels

Fatigue related problems in wheelsets have increased during the last 10-20 years, although total wheel damage related incidents in the same time have decreased in traffic [16, 17]. Fatigue is a threshold phenomenon, where the damage influence on a component level is related to actual load conditions and design factors [3]. Crack initiation often occurs at a point of high stress concentration, like an inclusion or surface defect. The propagation of the crack in subsequent load cycles will depend on the stress intensity and the inherent properties of the material. Controversially the increase of fatigue damage has been put forward to be an outcome of improved traction control systems and bogie performance together with development of steels with improved wear properties and thermal stability [17]. The magic wear rate [18], an expression of the beneficial counteracting process of fatigue crack growth by wear mechanisms on the tread surface, has therefore become difficult to at all times withhold. Increased rolling distance between maintenance and wheel reprofiling enables crack initiation and crack growth to be established as the wear is not sufficient to renew contact surfaces

In a wheel, the loads and fatigue mode may be assumed to be multiaxial on both component and material level [3, 19]. A good example is when the train is taking a curve, different curve radius between inner and out rail together with for example wheel slip and presence of cant deficiency can cause longitudinal and transversal loads simultaneous [3, 20, 21]. Commonly associated damage with curves is rolling contact fatigue (RCF) in the surface. RCF can be observed as a characteristic regularly spaced crack pattern all around the circumference of the wheel (Fig. 2.2). This damage type is one of the more common types of fatigue damage in railway wheels, related to excessive plastic straining of the material in the surface [3, 16, 22, 23].

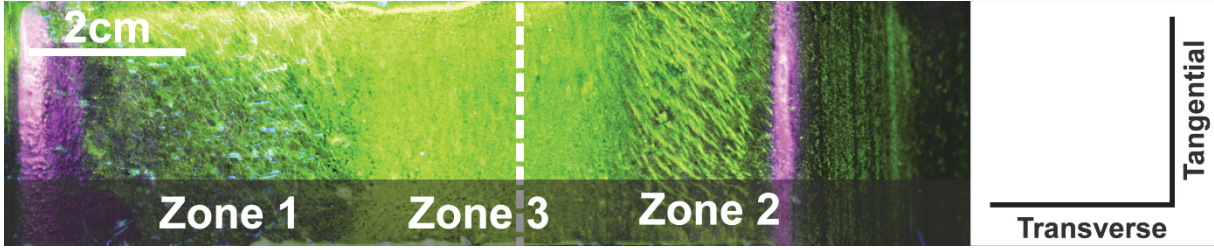


Fig. 2.2: Magnetic particle inspection of wheel tread surface section, the flange tip is on the right hand side of the image and the dashed line specifies the tread datum (70 mm from back of flange). RCF can be observed as regular spaced crack patterns at both sides of the tread datum. RCF in tread surface is typically referred to in three different zones.

For contact of a cylinder rolling on a planar surface, Hertz [24] stated the theory that the contact zone is elliptic with an ellipsoidal normal pressure distribution, valid for an idealised pure elastic system where no friction exists between bodies in contact, homogenous material and no presence of surface roughness. For a roll with radius R and pure line contact, the contact pressure p becomes,

$$p(x) = \frac{2P}{\pi a^2} \sqrt{a^2 - x^2} = \left\{ \frac{4PR}{\pi E} \right\}^{1/2} \quad (1)$$

where P is applied normal load per unit length, a the contact radius and E Young's modulus. The maximum contact pressure is found in the centre of the contact surface $p_{max} = 2P/(\pi a) = (4/\pi)p_m$. Maximum shear stress, $\tau_{max} = 0.3p_{max}$, exists below the surface at $x = 0$ and $z = 0.78a$ [25, 26]. This would suggest that largest shear stresses are below the surface, however influence of surface roughness and tractive forces in traffic causes the largest critical stresses typically to be located more in a thin surface layer [21, 27]. Therefore, for RCF the secondary factors like the rolling motion and surface irregularities have to be accounted for. As mentioned earlier, difference in contact velocity gives way for opposite strains in the two bodies with a resulting small displacement, i.e. a creep load [21]. Since the inner and outer wheel in a curve must travel a different distance, wheels are coned and typically arranged in bogies within each car to allow for some movement of the wheel axle connecting the wheels. This allows a smooth and steady curving at high speeds. Spin creep and two point contacts under such circumstances can develop as the flange is forced towards the rail while contact remains in the more central parts of the tread. Large lateral creep thereby can be generated, substantially larger than longitudinal caused by tractive forces [20, 22, 28, 29]. As a consequence (and further evidence) of the fact that the vehicle generates high creep forces in curves, surface RCF damage in rail track is found more often in curves than in tangential track and from observations of the wheel tread it can be seen that largest plastic deformation undergoes towards the edges of the tread surface [29]. RCF cracks may thus be assumed to initiate in the wheel tread due to the real contact pressure locally being several times over that of Hertzian smooth contact [27], resulting in accumulation of plastic deformation.

Subsurface crack initiation is possible as well due to Hertz theory and largest principal shear stresses existing below the contact surface according to equation 1, typically ca.

4 to 20 mm below the wheel tread [17, 22, 30, 31]. It has also been shown that cracks can initiate in the absence of initial material initiation point such as an inclusion, and be related to large plastic deformation and microcracking in the material [17]. Subsurface RCF may therefore be difficult to identify with commonly used non-destructive evaluation techniques during regular overhaul as they often have a rather large detection size limit. Subsurface RCF growth can become critical in service if rapid crack growth rate take place. Eventually such cracks may grow towards the surface and reveal themselves, leading to substantial loss of material in the wheel tread [3]. Subsurface fatigue cracking also implies that the lifetime of a wheelset is reduced as thicker material layers have to be taken away during reprofiling.

2.1.2.2 Material response to cyclic loading

Fatigue loading in general can be classified into two main groups, high cycle fatigue (HCF) and low cycle fatigue (LCF) [32]. Based mainly on cycles to final failure, or in other words, it is a result of the applied stress or strain amplitude that a component is subjected to. In HCF, the number of cycles to failure (N_f) are in the range of $N_f > 10^4$ and strains are purely elastic, while plastic strains are present in LCF giving a typical shorter lifetime, $N_f < 10^4$. When deciding for a suitable test evaluation method for wheel materials, a compromise has to be made. The many millions revolutions a wheel endures would suggest HCF testing. However, during running in of a new wheel surface, as well interpreting the increased load/strain amplitudes at defects and crack tips, LCF behaviour is often studied.

Pearlitic and most structural steels in fully reversed fatigue experience initially non reversible deformation associated with strain hardening that causes the material to harden or soften. This is valid in both strain-controlled and stress-controlled fatigue. It is known that microstructure and chemical compositions are some of the main determining factors. Precipitation hardened or soft annealing materials undergo hardening, while cold worked materials and quenched carbon steels in general experience cyclic softening [25, 33]. After the first cycles, a saturation level is reached as dislocation movement stabilises, resulting in a steady hysteresis loop where stress and strain amplitude are fairly constant until final failure [25]. In strain controlled fatigue testing of pearlitic-ferritic wheel materials, the third and final stage goes to completion fast [12] with a rapid decrease of stress amplitude, demonstrating that final crack growth is rapid.

Prediction and analysis of fatigue in a fully reversed load condition ($S_m=0$) with stress ratio ($R=-1$) can be estimated with reasonably good accuracy [34]. Evaluation and correlation of laboratory data with real fatigue behaviour of wheels are not as direct due to large plastic deformations, residual stresses, crack deflection events and mean stresses being far from zero etc. [2, 35]. Moreover, crack displacement in a wheel is taking place in mixed mode I, II and III, while in laboratory testing mode I is commonly used.

In wheel-rail design and evaluation, the term shakedown-limit is used to refer if a material remains in an elastic or plastic steady state during cyclic loading [21, 30, 36]. For steel under cyclic load four different general conditions, described in Fig. 2.3, can be present; (a) purely elastic load, (b) initial deformation with strain hardening resulting in purely elastic loading in further load cycles, (c) initial plastic deformation with strain hardening that after first cycles become fully reversible, i.e. LCF and (d) where build-up of plastic strain take place with each load cycle, i.e. ratcheting [3].

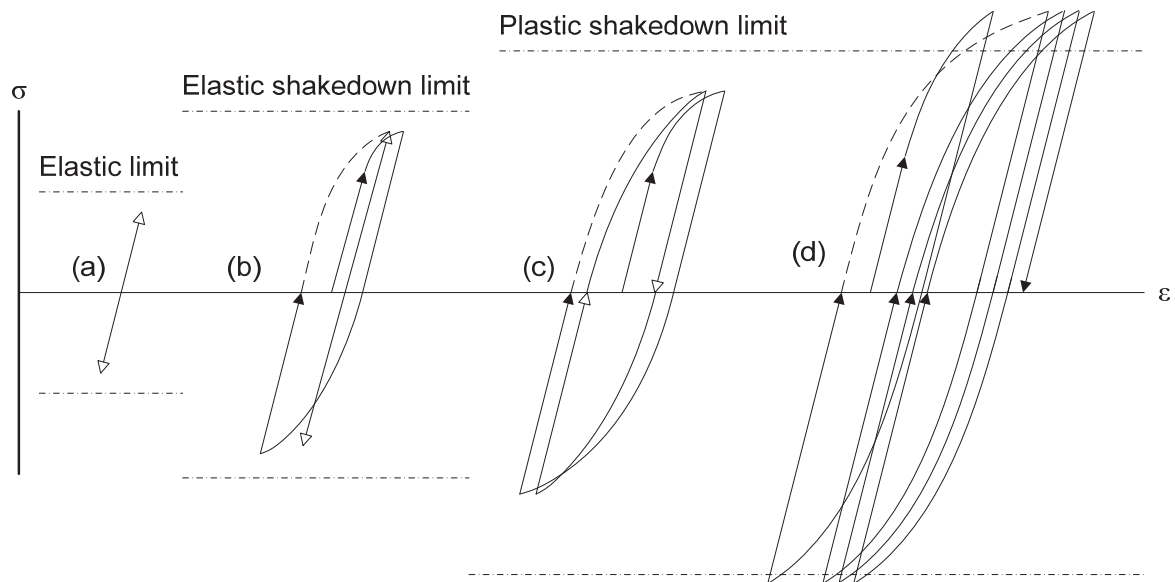


Fig. 2.3: Material response to cyclic loading (a) Purely elastic loading (below the elastic limit). (b) Initial strain hardening and elastic shakedown. (c) Initial strain hardening and plastic shakedown. (d) Cycle dependent creep, i.e. ratcheting, build-up of plastic strain with each load cycle ($R \neq -1$).

Plastic shakedown is the process whereby the material after initial plastic deformation will reach a steady cyclic state and no further deformation will occur [31, 37]. Thus, design and load predictions for cyclically loaded components should not allow such extent plastic deformation that the elastic shakedown limit is surpassed. If the limit is exceeded, the component can fail either due to low cycle fatigue (closed cycles of plastic strain) or by ratcheting which by accumulation of plastic strain causes a final ductile fracture [3, 31]. However, in wheel-rail contact, loading inevitably will go beyond the shakedown limit, confirmed by for example the presence of RCF in the tread surface. Wear will partially compensate for ratcheting by continuous material removal from the surface. If shakedown is reached or not is often depending on the deformation during the initial load cycles. An initial tribological geometric adaptation of the contact surfaces can increase the components load bearing capability and it will diminish further yielding in subsequent cycles, which may result in an elastic plastic steady state [38]. Work hardening counteracts the limit to be surpassed as residual stresses and strain hardening increase the yield stress, thus the shakedown limit rises towards higher loads, and a stable condition can be retained.

Good knowledge of material behaviour is needed in order to obtain better numerical models and predict different loading conditions related to the shakedown limit [2]. A problem lies partly within the high strain associated with ratcheting where fully reversible closed cycles of plastic strain are difficult to achieve in laboratory uni-axial testing [21, 30]. Since the strain required in the compression part of the load cycle is high, it can cause instability in the test specimen and after few initial cycles, failing by buckling is more likely than developed ratcheting. At present, twin disc testing have been successfully developed to simulate ratcheting and rolling contact fatigue [30, 39]. This approach implies that geometrical changes and especially wear will influence the evaluation. Moreover, drawbacks exist of inaccurate replication of true Hertzian contact, accuracy in determination of actual strains, scaling effects, environmental effects and high testing costs [35].

2.2 Materials for railway wheels

Pearlitic, medium to high carbon steels are the most common materials for railway wheelsets. Bainitic steels, which in some aspects have better mechanical properties than pearlitic steels, are also used to a limited extent. [35, 40, 41]. However, their performance in operation has not been successful until recent development of high carbon lower bainite grades. Unstable wear performance has limited their usage because of the difficulty to predict their wear rates in traffic. Even though many alternative wheel materials have been considered, pearlitic steels still offer the best trade-off between performance, predictability and cost.

2.2.1 Strengthening mechanisms of pearlite

The strength of pearlitic steels containing only a small amount of free ferrite is principally governed by the pearlite constituent while the ferrite phase influences mainly the ductility. The characteristic of each constituent can be alternated by careful selection of alloying elements and heat treatments. The strength of both ferrite and pearlite appears to follow a Hall-Petch type relationship for ferrite grain size and interlamellar spacing (ISP) respectively [42]. The Hall-Petch equation states the relationship between yield strength and grain size,

$$\sigma_y = \sigma_i + k_y d^{-\frac{1}{2}} \quad (2)$$

where d is a measure of mean grain size in ferrite and ISP in pearlite and where σ_i and k_y are material constants representing friction stress (Peierls stress) which opposes dislocation movement and dislocation locking [10]. The formula is derived from hindered dislocation movement by grain boundary refinement, resulting in increased yield strength. Gladman et al. further developed equations predicting material behaviour for medium to high carbon steels. Their work showed that the volume fraction of pearlite and ISP significantly affect both yield and tensile strength while ferrite mainly

influences yield strength. Therefore yield strength can be estimated as function of volume fraction of pearlite and ferrite [43],

$$\sigma_y = f_\alpha^n \sigma_\alpha + (1 - f_\alpha^n) \sigma_p \quad (3)$$

where σ_α is yield strength of ferrite, σ_p yield strength of pearlite and f_α volume fraction of ferrite. Values of n larger than 1 imply strain concentration in ferrite. The ISP of cementite lamellas is a function of transformation temperature, alloying content and to a limited extent on prior austenite grain size [44, 45]. ISP is inversely proportional to supercooling. Rapid cooling delays the transformation to lower temperatures, resulting in a larger volume fraction of pearlite and a refined lamellar structure. Yield and ultimate tensile strengths of pearlite may therefore be related to the reciprocal of the square root of ISP [46]. The influence of yield strength and grain size on fatigue, impact and wear behaviour, make control of pearlite morphology crucial in production.

2.2.2 Influence of alloying elements

Modern materials for wheelsets are made from vacuum degassed steels with accurate controlled chemical composition to minimize hydrogen content and formation of inclusions [22]. A characteristic chemical composition of a wheel steel grade commonly used in many parts of Europe is presented in Table 2.1. Since contact stresses between wheel and rail decrease, and traction increase, with increased size, wheels with large radius are preferred. On the other hand, large wheels impair the functionality of the passenger space therefore a compromise is made. Thereby, typical size of a passenger wheel diameter is close to one meter and has a weight of several hundred kilos; the total weight in a single train set being several tons. Even though the lifetime of a wheelset can be several years, the material cost is substantial and the use of expensive alloying elements is thus often limited. General influence of alloying elements is here discussed [16, 22, 47-49]:

Carbon controls the overall microstructure, strength, hardness, i.e. hardenability etc. and is the single most important alloying element. Increased carbon content raises solid-solution strength and increase the proportion of pearlite and, and in addition improves wear properties.

Manganese binds and helps to control sulphur which otherwise has an embrittlement effect on the steel. In similarity to carbon, manganese increases hardness and wear resistance by refinement of pearlite lamella and is often used to compensate for a decreased carbon content. Manganese enables in solid-solution strengthening and is a weak carbide former. The eutectoid reaction can occur at lower carbon levels and by so the amount of pearlite is increased. Toughness and work hardening behaviour are also improved which is important for maintaining strength in operation.

Silicon is a ferrite stabiliser and has a small influence on material strength by solid solution hardening. Having a negligible solubility in cementite, silicon has proven to inhibit cementite growth or precipitation and stabilises pearlite at exposure to high temperatures. Thus silicon helps to improve thermal stability and high temperature strength. While also improving wear resistance, too high alloying content may have an embrittlement effect and negative influence on impact properties. Silicon in the steel making process is used as a deoxidant to reduce oxygen and prohibits occurrence of iron oxide inclusions.

Molybdenum, chromium and vanadium improve wear resistance by formation of stable carbides and enhance strength and toughness. Chromium increases corrosion resistance and oxidation; in conjunction with molybdenum it increases hardenability and high temperature creep strength. Vanadium may be added to reduce excessive grain growth during heat treatments and thus promote a fine grained microstructure.

Residual alloying elements primarily take part in controlling and optimising the manufacturing process, improve cleanliness, grain refinement, and carbide formation. Their usage and amount may differ between different steelmakers but normally they are limited and specified in discrete intervals for each wheel grade specification to avoid unexpected material behaviour.

Table 2.1: Typical chemical composition of a medium carbon wheel steel grade in wt.%

C	Si	Mn	Mo	Cr	Ni	S	P	V
0.58	0.34	0.75	0.02	0.15	0.10	<0.001	0.010	<0.005

2.3 Microstructural degeneration

Heat treatment processes commonly used in wheel manufacturing involves normalizing, tempering, immersion quenching and rim chilling [12, 16], see also phase diagram in Fig. 2.4. Rim chilling, where the rim, tread and flange are cooled by water jets with subsequent tempering is widely adopted. A fine lamellar pearlite is obtained in the outer layers and allows the inner tread volume and wheel web to be chilled with reduced rate so higher ductility can be obtained.

Microstructural refinement and degeneration may however be considerable in operation. In the most outer millimetres of the wheel tread the material experiences large deformation and plastic flow. In a twin disc brake test Handa et al. [39] showed that within 100 μm from the surface, ultrafine grains with sizes smaller than 1 μm form, containing fine segments of fragmented cementite. Investigation of wheels from service in the current project showed similar results, in material that had undergone extensive shear deformation [29, 50]. Continuous dynamic recrystallization of ferrite grains [51] when high deformation is present, has been suggested as a possible thermomechanical

process where a fine grained microstructure can be formed [13]. Spheroidisation of cementite together with plastic deformation may also influence grain size, leading in similar ways to formation of such very fine grain structure in the surface of the wheel [48, 52]. The properties and appearance of such layers are in some ways similar to those of martensite, but the process in which they are formed are not same and hence further degenerative processes are probable to be different.

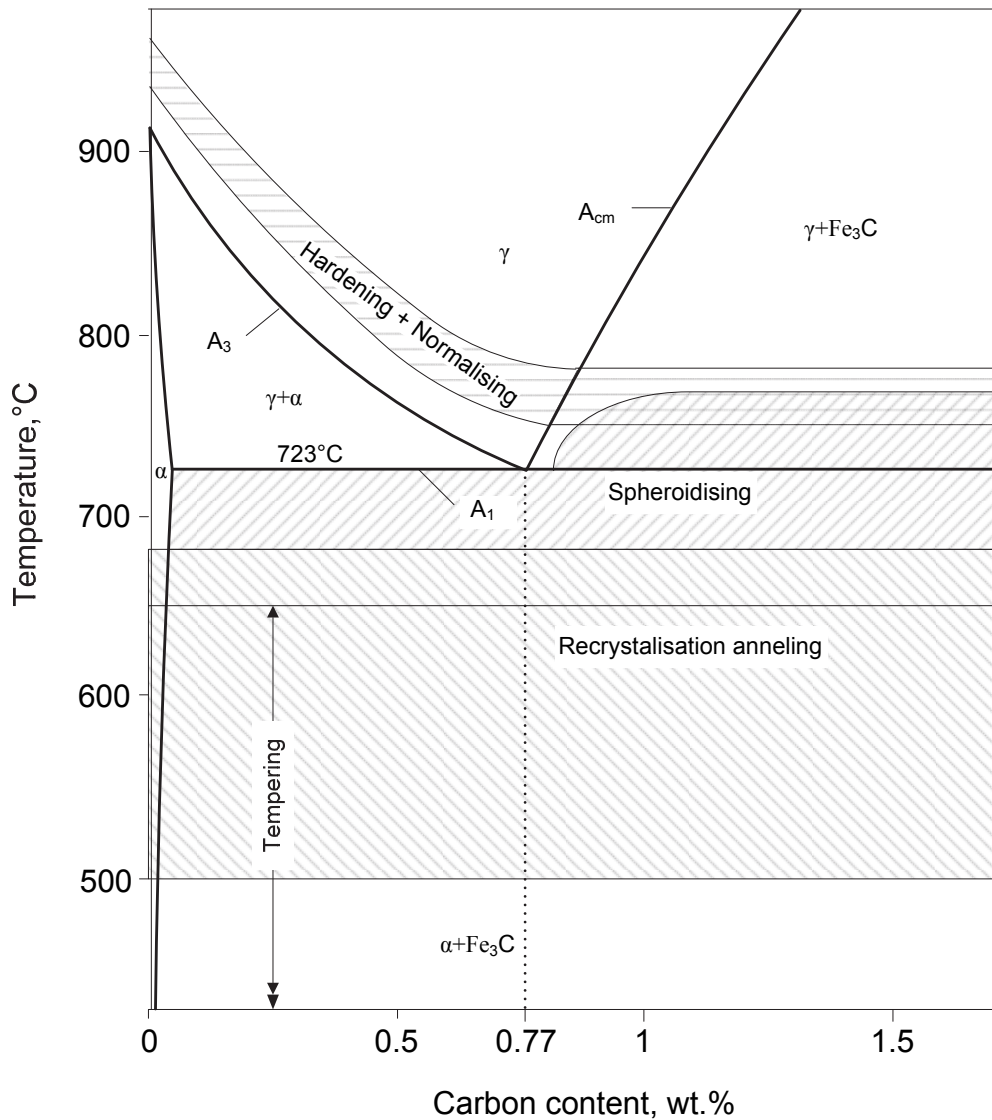


Fig. 2.4: Phase diagram of the iron-rich end of the iron-carbon system. For wheel manufacturing, common heat treatment process temperature regions are also included in the diagram.

2.3.1 Recovery and recrystallization

When a metal is plastically deformed, most energy is dissipated as heat, but a small percentage will be stored within the material as dislocations, point defects and surface energy in grain boundaries interfaces. For the case of deformation and annealing processes in metals the contribution from dislocations is the main significant source of the stored energy, reaching densities as high as 10^{17}m^{-2} in severely cold-worked metals

[51, 53]. Stored energy is typically released gradually during heating. Initially, for low temperatures, the changes in mechanical properties may be small and effects on microstructure can be difficult to observe with light optical- or scanning electron microscopy. It is when the temperature reaches so high that recrystallisation and or grain growth proceeds, such analysis methods become more useful. To capture the process, transmission electron microscopy, X-ray diffraction, resistivity measurements or calorimetric may be used instead. For processes where a combination of high thermal and mechanical load exists, deformation can occur concurrently with softening mechanism, i.e. dynamic recovery and recrystallization. An important aspect of dynamic recovery and recrystallization is that plastic deformation and stresses may increase the process rate [51, 54, 55]. A fundamental distinction in the on-going process between recovery and recrystallization is made by if low- (LAGB) or high (HAGB) angle boundaries are affected, where a grain boundary misorientation of more than 10-15° normally is defined as HAGB. Recovery is mainly related to dislocation and boundary movement of LAGB whilst recrystallization and grain growth concerns HAGB [51].

Recovery takes place for lower temperatures, at analogues temperatures $\left(\frac{T}{T_m}\right)$ of approximately 0.4 to 0.5 of the melting temperature. In plastically deformed metals recovery take place by annihilation and rearrangement of dislocations, involving several microstructural events [51, 55]. The process is gradual and takes place over a large temperature range. Changes in mechanical properties after and during recovery can be observed as a decrease in yield stress and hardness, when the dislocation density decreases [51].

At higher analogous temperatures, typically over $0.7 T_m$, recrystallization occur, with a much higher rate than that for recovery. Recrystallization will be dependent on characteristics of the thermal cycle, a slow annealing process with a low heating rate, allows for more energy to be released at low temperatures. Recovery has a lower activating energy, therefore affecting the grade of recrystallization [51]. Recrystallization takes place by nucleation and growth of newly created grains, and may be observed with optical microscopy when the process is allowed to undergo far. Similar to recovery, a large deformation, i.e. high dislocation density, will accelerate the process and also a smaller initial grain size. Softening will also be present for recrystallization, but in order to have detectable effects much less time is needed, a few seconds at high temperatures. For dynamic recrystallization the process can be reduced to even shorter times [54]. As new grains are nucleated and primary recrystallization is complete further grain growth can undergo if the temperature is kept high. Remaining surface energy after recrystallization in the grain boundary can provide a thermodynamical driving force for a more ordered grain configuration to be attained whereby further grain growth can take place [54, 55].

2.3.2 Spherodisation of cementite lamellas

In pearlite, bainite or tempered martensite, cementite within the primary structure may break up and coarsen by a spheroidising process [53], influencing yield and ultimate tensile strength according to the Hall-Petch relationship, see Fig. 2.5. Spheroidisation of pearlitic microstructure can occur both in rail and wheels in operation and has also been identified in laboratory twin disc tests [52].

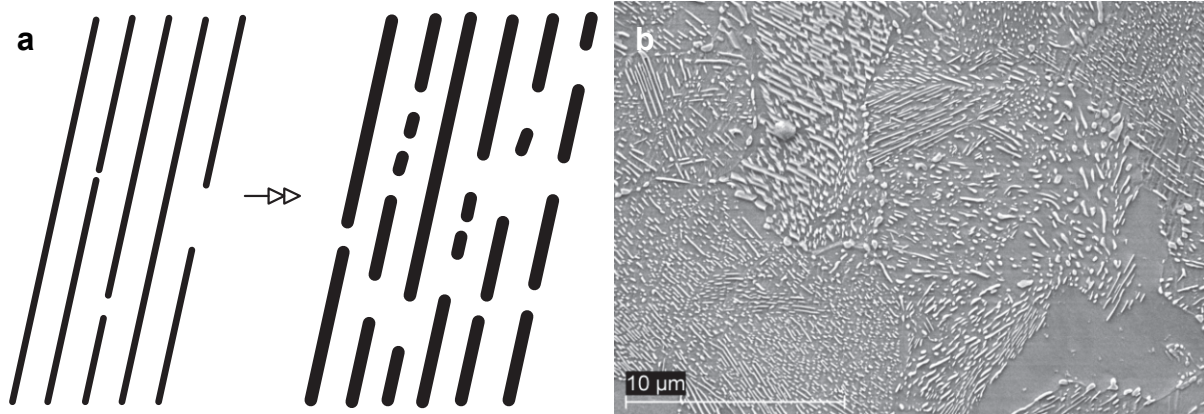


Fig. 2.5: Spheroidisation of pearlite. Morphology change appears as reduction in lamellar length and increase in lamellar thickness. With increased exposure time/temperature/deformation carbides gradually evolve into spheroids. (a) Schematic sketch, and (b) scanning electron micrograph of spheroidised microstructure.

The alloying elements Cr, Mn and Si efficiently reduce ISP and retard further coarsening of cementite particles and lamellas at elevated temperatures [48, 56, 57]. In particular Si, which is a ferrite stabiliser non-carbide forming element, that dissolves exclusively into the ferrite but may enrich in cementite or at cementite-ferrite interfaces due to the non equilibrium formation of pearlite from austenite. Upon annealing cementite degeneration is slowed down, in particular at temperatures between 400 and 600°C. Retardation of coarsening is considered to be due to an increased activity of Si around growing carbides. A saturated layer of Si reduces flux of C onto the carbides [57]. Also with increased alloying content, more Si will be found in or around the cementite lamellas as the carbides will form at a lower temperature in manufacturing, as shown in Fig. 2.6. Manganese, weak carbide former has a similar retarding effect as Si but at higher temperatures [48, 57].

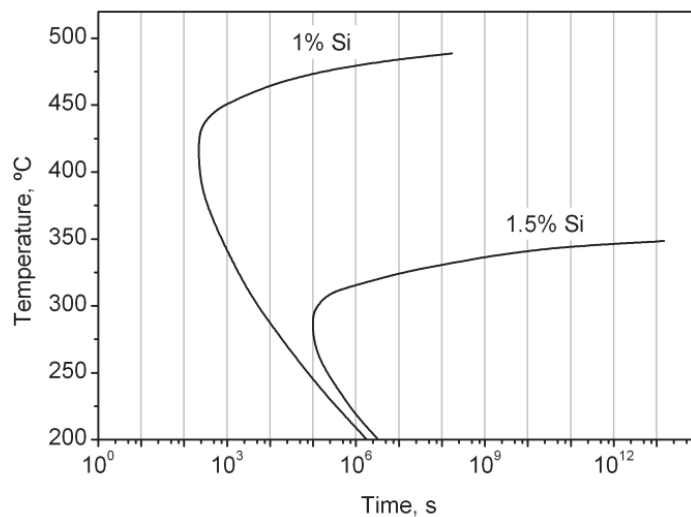


Fig. 2.6: Time temperature precipitation diagram for cementite in a system of Fe-Si-Mn-C, (Fe-1.2C-1.5Mn-1.5Si) adapted from Kozeschnik et al. [58]

2.3.3 Martensite formation and tempering

The notation martensite in metallurgy generally stands for a diffusionless processes where all transforming atoms are displaced simultaneously [59]. For steels the transformation principally takes place athermally and the hardenability is mainly a function of the carbon concentration. Depending on the crystallographic order, the transformation is virtually time-independent with rapid nucleation and growth [60]. E.C. Bain proposed the nonexistence of diffusion and a homogeneous process where the crystal structure is altered, from the austenite fcc lattice to bct, with deformation of the crystal cell, i.e. change only of the length of lattice parameters. It is now known that twinning or slip also must take place of the crystal units to facilitate the transformation and that a heterogeneous behaviour is likely [53, 61, 62]. Alternation of the crystal lattices results in a global dimensional change with increased volume, often associated with internal strains and risk of cracking. The amount of transformed martensite is governed by the undercooling in connection to the martensitic start and martensitic finish temperatures. During nucleation the initial nucleus is coherent with the austenite and nucleation initiates mainly at positions with structural defects in the lattice. In martensite, contrary to the diffusion nucleation process, the influence of strain energy is larger than the surface energy. External stress or deformation of the crystal structure prior to a martensite transformation thereby also may ease transformation to proceed. The growth is a rapid process with grains forming as fast as 10^{-7} s^{-1} , grains preferably growing as small thin plates in order to minimize the strain energy along preferable planes, denoted habit planes. The final microstructure in steel will normally consist of non-ordered martensitic plates together with a few percentage of austenite, i.e. retained austenite, which did not transform during the process [62].

The iron-carbon martensite structure is unstable and already for moderate heating will start to decompose into more stable phases. Tempering of martensite involves several

microstructural transformations, resulting typically in decreased strength and increased ductility. There are a few established main tempering stages commonly defined in the literature for medium carbon steels [61, 62]. Temperature intervals for the different stages are denoted, but may vary depending on specific alloy composition and heat treatment, different process can also undergo simultaneously. Up to 200°C, the excess carbon in supersaturated martensite segregates out from the solid solution. The distortion of the lattice by dislocations and cell walls provides sites with lower energy than interstitial positions, therefore carbon atoms will segregate to, or form clusters around these defects to lower their chemical potential [63, 64]. High dislocation density makes possible the movement of carbon atoms close to room temperature, hence segregation may take place already during the initial quenching process, i.e. autotempering [63, 65]. Around carbon rich sites eventually ϵ - or η -carbide nucleates. Between 200 and 300°C any existing retained austenite transforms to ferrite, cementite or bainite. From ca. 200°C to 350°C, the full tetragonality of martensite is lost and a structure of cementite and ferrite is obtained. The carbon content in the martensite decreases and complete transformation occurs from bct to bcc lattice structure. Cementite precipitates fast, with ϵ -carbides, twin- and grain boundaries serving as nucleation points [61]. At higher temperatures and longer tempering time, cementite coarsening, recovery of dislocation substructure, spheroidisation and formation of alloy carbides may take place. During tempering the reverse volumetric process, with a shrinkage will progress. The attributed shrinkage in volume, when martensite loses its tetragonality, can also be used to identify different stages of tempering, apparent as dilatation effect in dilatometry trials [61, 66, 67]. As the initial tempering stages involves short range carbon diffusion distances they can proceed fast [61]. Higher carbon content yields for example higher hardness, but upon tempering the softening rate will initially be higher when compared to steel with lower carbon content.

3 Experimental techniques: details and theory

3.1 Microstructure evaluation

Ability to set relations between microstructure and mechanical properties is essential for obtaining a universal profound deep knowledge, and an accurate prediction of mechanical properties. However, the nature of the imaging analysis process for microstructural evaluation itself may give errors that can influence the results even for large sample sizes. Consequently the true material behaviour and composition in some cases may be unattainable solely by image analysis. Mechanical testing often gives a superior global averaging of mechanical properties.

Microstructural characteristics of grain size, phase fractions, morphology and fracture surfaces were analysed using standard metallographic techniques with a Leitz DMRX light optical microscope (LOM) and stereo microscopy, Zeiss SteREO Discovery.V20. The software AxioVision v.4.7 (Carl Zeiss) was used for image analysis. For microscopy metallographic preparation by SiC grinding, polishing and etching was used in general. As the last polishing step, chemomechanical polishing with SiO₂ (colloidal silica) was used instead of traditional abrasive diamond polishing. By using chemomechanical polishing, the quality of prepared surfaces improved, which allowed for a more accurate evaluation of for example the cementite lamella morphology in pearlite. In order to reveal the microstructure etching was performed with Nital solution (2-3 % HNO₃ in ethanol).

Shear strain anisotropy in the tread surface of the wheel was also studied with LOM. By use of the tangent α method, plastic flow as function of depth was determined [68, 69]. The precision in the analyses depended on the quality of micrographs and detectable microstructural features. When the measured shear angle increases typically the analysis accuracy increase as microstructural features are easier to perceive. The mathematical expression used for the shear strain yields that highest measurement sensitivity exists in the calculated value for large angles.

Scanning Electron Microscopy (SEM) offers a higher spatial resolution and wider magnification range than LOM with retained or even better depth of focus. In-lens secondary electron (SE) and backscatter detector (BSE) were used, where BSE offers a quick way to distinguish different phases by means of atomic mass influencing number of BSE electrons reaching the detector. The instrument used was a LEO 1450VP. In addition to general investigations of different microstructures and cracks the SEM was used for determination of cementite ISP corresponding to the minimum apparent spacing, λ_0 , measured perpendicular to lamellas within pearlite colonies having the shortest spacing within a random polished plane [70]. Initial evaluation of third body material observed in cracks was made with BSE detector to establish if the material was similar to the base metal or not.

3.2 Mechanical testing

Cyclic and monotonic tests were performed in a servo-hydraulic INSTRON 8032 rig (50 kN load cell) in a closed loop control system with 1 kHz sampling rate. Push-pull, completely reversed ($R_\epsilon=-1$) LCF tests were made at room temperature. Accurate alignment of the grips was performed prior to testing to minimize bending stresses. Tensile tests were made for different strain rates and temperatures by the use of a climate chamber. Fatigue and tensile tests were both made in strain control condition by use of a clip-on strain gauge extensometer. However, load control was used for compression tests, primarily due to the risk of the extensometer knives slipping on the very hard martensite specimens which could lead to a large and rapid response of the machine, damaging the test fixture. Compression tests were performed in an IITRI compression test fixture (ASTM D 3410 standard) mounted in the servo-hydraulic rig. A climate chamber and resistive heating was used to enable simultaneous heating during loading in compression, similar to thermomechanical loading in a Gleeble test machine. In compression, samples start to buckle typically around at L/D ratio of about five. As maximum power was limited to 4kW this also limited the specimen sizes. In order to reach temperatures up to 400C° with heating rates close to 200K/s, the largest cross sectional area possible to use was around 3mm². Strain was measured with a modified clip-on extensometer, 3.5 mm knife blade gauge length and blades electrically insulated from each other.

Charpy V-notch impact tests were carried out according to European EN 10045-1:1990 standard, by use of a VEB Heckert 423/17-1980 equipment. Specimens were liquid cooled in alcohol or heated in a conventional oven. Impact energy was measured and the brittle to ductile fracture area ratio calculated afterwards by evaluation of the fracture surfaces.

Vickers indentation was performed with a Wolpert Testor 7021 machine for macro hardness and a Shimadzu HMV-2000 for micro hardness using standard techniques [71, 72]. Care was taken to avoid induced deformation in the sample preparation, as a minimum for macro hardness grinding to 800 grit and for micro 3µm diamond polishing was made.

3.3 Residual stress measurement

X-ray diffraction (XRD) technique is a commonly used non-destructive method to evaluate crystallographic configuration and quantitative residual stress state in components close to the surface. X-ray stress analysis relies upon identification of the small changes in interplanar spacing of crystals which takes place due to elastic straining. The essential parts of a measurement equipment is an X-ray source and an electronic detector, as a Geiger counter, which can record the X-ray reflections [53]. When the incident angle towards the specimen is altered, by rotating the goniometer (X-ray and detector assembly), the X-rays interact with the crystals in the material, the

diffraction and reflection angle can thus be determined according to Braggs Law [73]. The reflected intensity is obtained as a function of Bragg angle. By using the $\sin^2 \Psi$ method, presence of elastic residual stress can be detected as a shift of the diffraction peak, i.e. a change in angular position, while the beam angle is shifted by an angle Ψ , the magnitude of the shift and knowledge of the Young's modulus and Poisson ratio of the material will enable a determination of residual stresses. Retained austenite can be obtained by determination of the diffraction intensities of different phases, like ferrite, martensite, austenite etc., the integrated intensities obtained represents the volume fractions of each phase which then can be calculated [74]. Residual stress measurements were performed using an Xstress3000 diffractometer with Cr K_α radiation, 1 mm diameter lens on the goniometer. The same equipment, with altered detector configuration and Vanadium K_β blocking filters was used to measure retained austenite.

3.4 Dilatometry

Dilatometry is a technique used to measure dimensional changes of solids and to analyse solid state kinetics [75]. In the current work, the linear thermal expansion coefficient (CTE or α), was recorded during heating and respective cooling, for pearlite and martensite microstructure. The linear thermal expansion is defined as

$$\alpha_l = \frac{1}{l_o} \left(\frac{\partial l}{\partial T} \right)_F . \quad (4)$$

The subscript F indicates that the samples is kept under a constant force during the measurement [76]. This force is low and needed only to have continuous contact with the sample. To determine the CTE profile, displacement and temperature are measured while the specimen is undergoing a thermal cycle [77]. In the current study a pushrod dilatometer of type Netzch DIL 4012C was used, where the specimen is placed on a carrier; in one end the specimen is fixed and at the other end the pushrod is in contact with a constant force. A transducer connected to the pushrod allows for accurate measurement of the change in sample length and a thermocouple placed in close proximity to the specimen measures the actual temperature during the thermal cycle. Silica (Al_2O_3) having low stable and well established thermal expansion was used as calibration material. Usage of low heating rates during testing, improve temperature homogeneity within the specimen and also gives longer time for phase transformations to progress completely, thus increasing accuracy in capturing of dilatation effects and temperature control.

3.5 Differential scanning analysis

Differential scanning calorimetry (DSC) is a thermal analysis method that measures heat capacity (C_p) as function of temperature and heat flow [78]. Two common types exist, heat flux and power compensated DSC. While having different measurement configuration, they both enable the difference in heat flow of a specimen to be measured in comparison to a reference during continuous heating and cooling [76]. Generally the

reference is an empty sample holder, i.e crucible, utilized to compensate for the heat flow of the crucible containing the actual specimen. Temperature of the sample and reference are measured continuously by a differential thermocouple in contact with the sample- and reference crucible [76].

Reactions involving a large change of heat flow, like for example melting, can be observed as endothermic or exothermic dilatation effects in the resulting measurement curve. Melting and solid state kinetics, in similarity to dilatometry thereby can be studied [76, 78]. Some transformations involve only small energies, and are therefore harder to identify, as for example recovery in steels. A technique to overcome such problems is to run the same specimen for two consecutive runs [79, 80]. Differentiation of the heat flow from the first and second run thereby enable measurement of very small changes in heat flow. This assumes the reaction has time to proceed during the initial run and noise or concurrent processes like oxidation, don't overlay the actual reactions.

3.6 Auger electron spectroscopy

Auger electron spectroscopy (AES) was used to study apparent residual debris in surface and subsurface cracks. AES as an analytic technique to examine chemical composition has the benefits to provide a precise analysis within a very small volume. In the current work a ThermoScientific Microlab 350 instrument with a lateral resolution down to 12 nm nominally was used. The lateral resolution was required, as the characterisation of crack residuals containing metal particles and oxides showed a multi-level lamellar structure down to a submicron level.

When the specimen is exposed to an electron beam, the electrons interacting with the atoms can result in an ionization process, where a core hole is created. The vacancy will immediately be filled by an electron that relaxes from an outer shell. This can result in emission of an X-ray photon (used in X-ray spectroscopy), or alternatively a second outer shell electron can be ejected, i.e. an Auger electron. Accordingly, the reaction involves three electrons; one being ionized, one outer shell electron filling the core hole and the auger electron being ejected from an outer shell [53, 81]. The kinetic energy of the Auger electrons are specific for each element and independent of the incident beam energy. But the energy associated with the Auger electron is low, hence only emission from atomic interaction in the most outer surface layer (a few nm) will be able to reach the detector. Therefore, as the effective detectable interaction volume is small a detailed surface analysis can be obtained.

The surface sensitivity of the analysis technique also demands high cleanliness of specimens and usage of ultrahigh vacuum in the chamber in order to avoid contamination and deposition of monolayers on the specimen surface. Wear debris present in examined cracks, and contamination from the specimen preparation which had got captured within cracks and cavities in the surface, therefore made the analysis difficult. Under the high vacuum in the instrument, the contaminations migrated out to

the surface of the specimens. Only a short time span therefore was available for the analysis to be performed after cleaning the surface with ion etching, before the surface would get contaminated again.

3.7 Heat treatment

Long-time annealing trials were performed in a tube furnace with a protective argon atmosphere to prevent decarburization. The temperature was measured with thermocouples placed in the centre of the furnace and within a reference sample. In this way, it was possible to measure the interior temperature development. The complete temperature stabilisation when heating up to ca. 500-700°C took around 2-3 minutes for specimens of a few millimetres in size.

Laser heating was used to simulate a local rapid thermal heating process within a larger material volume. The technique allows for a precise control of heating time within a focused small surface area. As the heated volume compared to the whole specimen volume is small, high cooling rates also are obtained after the laser is turned off. A 2.8 kW diode laser was used for irradiation of specimens within a vacuum system. The laser radiation was guided via an optical fibre and defocused to a diameter of 6 mm at the sample surface. Temperature in the innermost 2 mm diameter of the laser spot on the exposed surface was measured with a pyrometer, sampling frequency 60 kHz.

Resistive heating techniques enable fast and more homogenous heating of larger material volumes in comparison to laser or induction heating, where the work piece is primarily heated from the surface in towards the core. When heating time is short and no forced cooling is applied, the heat convection from the surface has small influence and can often be neglected. Gradients thereby are small in a perpendicular cross section to the electrical field, but since the specimens typically need to be fixed in some kind of holder, gradients will usually exist along the sample towards the fixture. In the current study, resistive heating was primarily used as a method to study influence of pearlite and martensite tempering while subjecting the test sample to an external constant load. As current source a digitally controlled DC power supply of type SM 15-400 (Delta Elektronika) was used, with a power output up to 4kW.

3.8 Temperature measurement

Measurements of temperature, in the contact area between wheel and rail in railway traffic, and in laboratorial experiments for short heating times are challenging. Therefore often different techniques are needed accordingly to obtain the true temperature field.

Thermocouples allow for measurement of temperature within a wide range, typically from close to absolute zero up to about 2000°C [76, 82]. A thermocouple is made up of two different materials with different electrical resistivity-conductance. When

connected and elsewhere isolated electrically from each other, a small but measurable electrical signal is created when the junctions (thermoelement and terminus junctions) are kept at different temperatures. The heat flow between the junctions, is governed mainly by electrons and it is proportional to the temperature gradient giving a net electrical current flow (Seebeck effect), i.e. an electromotive force (EMF) which can be measured [76, 82, 83]. In order to have good heat conduction the thermocouple is generally welded to the specimen. Therefore, the size of the wires, weld bead and grounding influence the measurement accuracy and the response time [82-84]. A small junction (small thermal mass) results in a faster response, and so does grounding, i.e. mechanical contact of the wires directly to the specimen measured. Still, the measurement technique is typically limited to heating times longer than a few tenths of a second or so, due to thermal lag (i.e. stabilisation of thermal gradients).

Moreover, contact with the specimen may not always be possible and welding can alter the properties around the weld point. With non-contact pyrometric measurement techniques such problems can be overcome. Pyrometers offer a high sampling rate, sensitivity and extended measurement range but also a decrease in absolute temperature accuracy compared to contact measurement techniques [82]. When a material is heated, electromagnetic waves are radiated. By measuring the intensity, the temperature of the emitting body can be determined. According to Wien's law, the wavelength of thermal radiation is shifted towards shorter wavelengths and the total intensity rises when temperature increases [84]. This assumption is valid for a blackbody, i.e. a physical body that absorb all incident electromagnetic radiation and re-radiates energy independent of shape and incoming radiation. Many materials though, like metals, do not have true black body behaviour. The emission coefficient (emissivity ϵ , 0-1) is used to describes emission from a real object compared to the idealised black body [82]. When heating a metal, i.e. a gray body, the emission coefficient will not be constant as emissivity is wavelength dependent, and surface reactions like for example oxidation may influence additionally. Heat radiation is detectable by the human eye at higher temperature, when the material starts to glow within the visible wavelengths (ca. 0.4 to 0.7 μm), however highest intensities are present in the infrared range detected as heat radiation [76, 84], thereby solid state infrared detectors can be used to measure temperature [85]. Two main detector classes are common, photon (quantum) and thermal detectors. For a photon detector incident photons hitting an IR sensitive semiconductor generates an electrical charge, while in a thermal detector the absorbed IR radiation causes a temperature change of the detector material which is measured by secondary techniques, for example by resistivity [82, 85]. Use of two colour pyrometry (ratio pyrometer) in theory can eliminate the problem with that the emissivity often is not constant. If the change of emissivity for a material is assumed to be equal at different wavelengths, measuring the object at two different wavelengths simultaneously enables the absolute temperature to be determined independently of the emissivity by calculating the response ratio [84]. Nevertheless, metallic surfaces have a very low emissivity compared to non-metals and if the emissivity is non-linear within

the present spectral range (grey body behaviour), small errors may be still present in the measurement [84].

In this work thermocouples were used where a stable temperature had to be measured, like in the oven heat treatment trials etc. Mainly K type (nickel based) thermocouples were used; due to their wide temperature range and relative low cost. In order to have fast measurements with low lag time, pyrometers were utilised in the laser and the restive heating experiments. For the resistive trials, the samples were covered with a surface modifier (hydrocarbon soot), having a constant and know emissivity, allowing usage of a compact and simple handheld measurement equipment. The method and accuracy was validated by performing calibration with samples having attached thermocouples.

3.9 Materials

Two pearlitic wheel steels grades with a slight difference composition were used in this investigation. The R8T wheel grade (corresponding to European ER8) defined by the EN13262 standard [16] and a second higher alloyed grade with 1 wt.% silicon and 0.95 wt.% manganese, here and in the appended articles denoted as HiSi. The nominal chemical compositions are given in Table 3.1. In production, wheels have treads and flanges rim chilled, giving a finer pearlitic microstructure close to the tread surface. Material for testing was extracted from wheels in their unused virgin initial state and from wheels which had been used in service, both with and without apparent damage.

As often common in manufacturing of components, the large bulk material volume and consecutive heat treatments during manufacturing results in small variations. For most wheel steel grades the chemical compositions and mechanical property levels are defined in specific ranges for different markets and applications. Variations of a few percent for example yield and fracture strength can therefore exists between different batches, being accepted as long as the values are within the standard values. The used materials showed small variations in the initial mechanical properties, but they were confirmed to be within specification grade. However, relying only on absolute values of mechanical data could lead to a non-truthful understanding of the material properties. Effort therefore was put on understanding underlying behaviour factors and trends of measurement data. Correlation of hardness to strength and fatigue life showed to be one good method to relate the test results with the initial properties of test samples.

Table 3.1: Chemical composition of materials in wt.%

	C	Si	Mn	Mo	Cr	Ni	S	P	V	Fe
HiSi	0.57	0.99	0.95	0.04	0.14	0.12	<0.001	0.008	<0.005	96.9
R8T	0.58	0.34	0.75	0.02	0.15	0.10	<0.001	0.010	<0.005	97.8

As shown in Fig. 3.1, where hardness mapping of the rim cross section of a virgin wheel is displayed, hardness varies both radially and transversally. Since the values varies from approximately 250 to 305 HV10 over the cross section, the position of the extracted specimens from the wheel can have an influence on the experimental results if care is not taken. This being even more important in used wheels where stronger gradients can exist. The free ferrite content was found to be 5 to 10 vol.% and the grain size ranging from ASTM No. 7 to 8.5 measured 15 mm below the wheel tread surface in a central position.

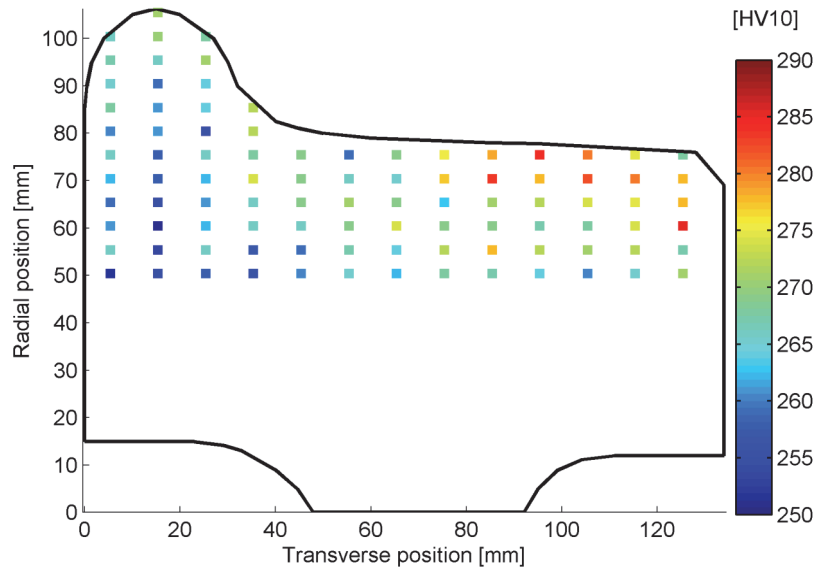


Fig. 3.1: Hardness mapping on the cross section of a wheel rim in its initial state. Observe the hardness gradient from the tread and flange towards the wheel web, owing to rim chilling in manufacturing.

In Fig. 3.2 LOM and SEM micrographs of the examined pearlitic-ferritic steels show the pearlite morphology. The overall composition and pearlite morphology are fairly alike, with alternating regions of mainly pearlite and free pro-eutectoid ferrite. The tread layer in used wheels obtained from service can have a broad variation in mechanical and microstructure properties. Vehicle type, bogie position, track layout, reprofiling and weather conditions are just a few of the parameters that will influence. Therefore the study of used wheels, real damage cases and track tests often enables a more realistic approach and provides knowledge needed to understand and develop laboratorial trials and advanced twin disc rig tests. However again, cost can be an important decisive factor. In this work used wheels proved to be important for characterisation of the actual microstructure, to obtain material with high plastic deformation and to examine properties of propagating cracks. Since the microstructure in the tread surface layer of a wheel undergoes vast plastic deformation, the microstructure is much different than the initial microstructure shown in Fig. 3.2 [29].

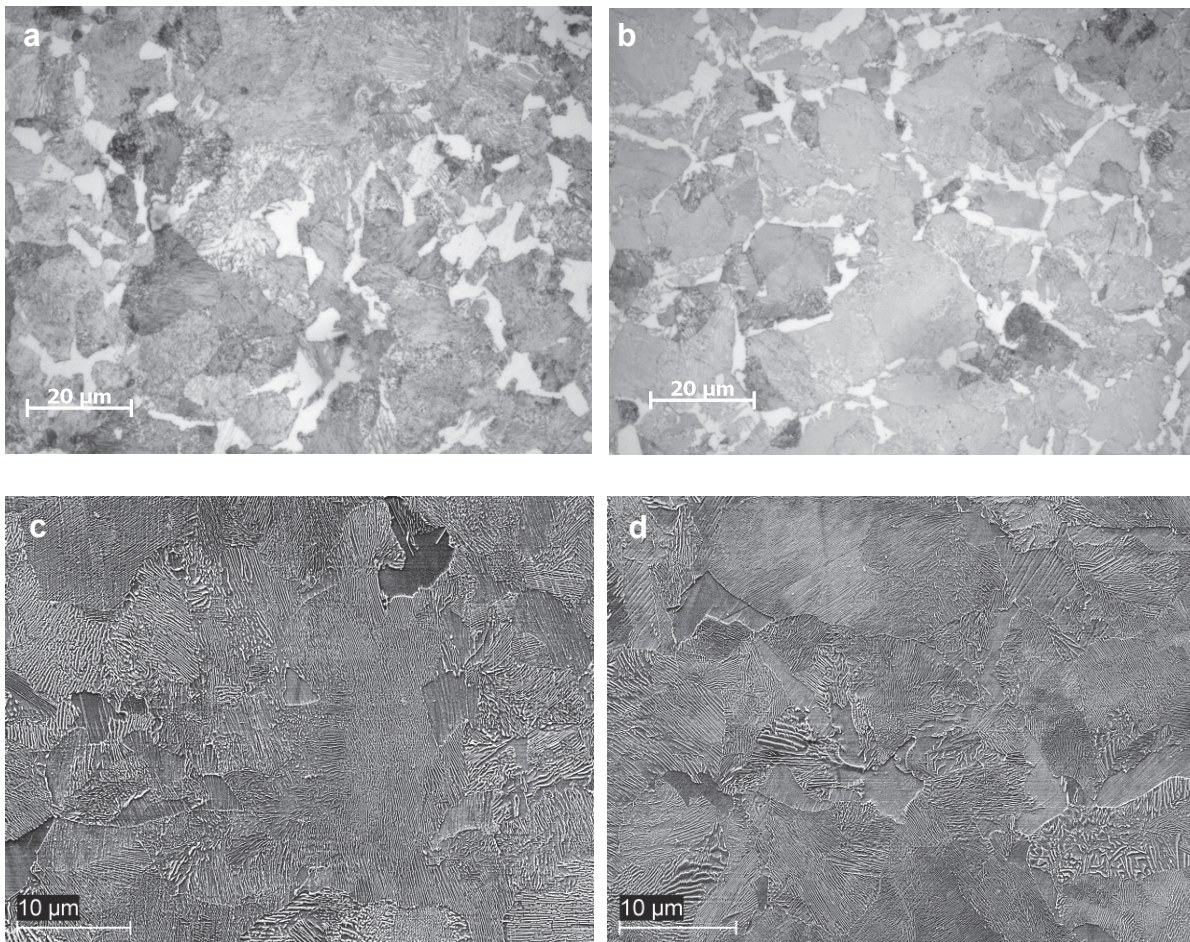


Fig. 3.2: Micrographs of pearlite-ferrite structure. In (a) HiSi initial state and (b) R8T initial state LOM at 500x, light etching phase pro-eutectoid ferrite and dark constituent pearlite. In (c) HiSi initial state and (d) R8T initial state SEM at 5000x, dark etching phase pro-eutectoid ferrite and lamellar/mixed grey constituent pearlite.

3.10 Material extraction

All samples for mechanical testing from virgin wheels were extracted approximately 15 mm below the tread section along the running direction, see Fig. 3.3. Since the samples had a fairly small cross section, variations of material properties in radial and transversal directions within a single specimen were considered negligible. LCF and tensile test specimens were machined into cylindrical bars with a gauge section of 6 mm and 11 mm grip section (Fig. 3.4). To reduce surface defects and residual stresses from machining, the gauge sections were carefully ground and polished in several steps to 4000-grit, until a mirror like surface was obtained. From the same material as used for LCF specimens, dilatometer samples were made, with cylindrical rod shape 50 mm long and 6 mm diameter.

Samples for compression testing were machined in their perlitic state. Martensite structure was obtained by austenitisation at 900°C and then quenching to obtain a fully martensitic microstructure. Care had to be taken not to induce any plastic deformation

during extraction and forming of the samples, which otherwise could affect the test results. The samples were about 8 mm long and 3 mm in diameter.

For laser tempering, coin-like specimens with a thickness of 3mm and diameter of 22.5 mm were machined. In order to have uniform laser radiation absorption in between different specimens, the surfaces were polished with 3 μm diamond suspension.

In Fig. 3.5 the specimen geometry for Charpy impact testing is shown. The V-notch (root radius 0.25 mm) was orientated towards the tread.

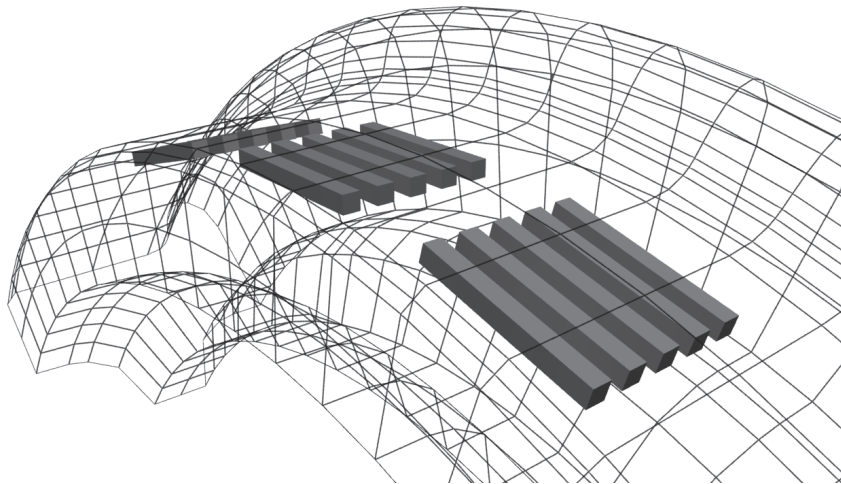


Fig. 3.3: Position of samples for LCF, tensile and Charpy impact tests. All samples were extracted approximately at a depth of 15 mm below the wheel tread.

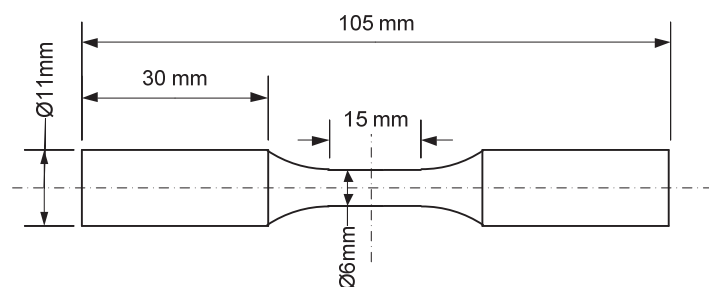


Fig. 3.4: Geometry of low cycle fatigue and tensile test bars.

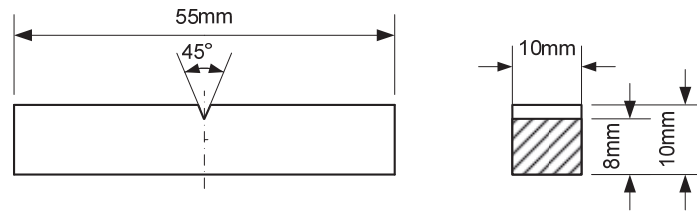


Fig. 3.5: Geometry of Charpy V-notch impact tests (notch radius 0.25 mm).

4 Summary of results

This section presents a selection of the main results and analysis. For more detailed results and discussion the reader is referred to the papers appended to this thesis.

4.1 Influence of alloying content on stress-strain behaviour

In paper I, two wheel steels with different chemical composition were investigated. One reference material denoted R8T and a second one with increased silicon and manganese content, denoted HiSi. Tensile tests performed from -60 to 180 °C together with LCF testing showed that initial material properties at room temperature dominated the material response. In the first test batch of wheels, the R8T material had a slightly higher hardness compared to HiSi, 305 compared to 280 HV10. Consequently in monotonic testing the R8T material demonstrated a higher yield and tensile strength as seen in Fig. 4.1(a). However, the flow stress of the HiSi material is less temperature sensitive than that of R8T. Overall, the difference in chemical compositions between the materials proved to have a limited influence on the monotonic stress-strain development. In paper II, the chemical composition was seen to influence monotonic properties when the materials were initially annealed at a temperature just below A_1 prior to testing. The heat treatment resulted in a decreased yield and tensile strength Fig. 4.1(b), but the results showed that HiSi soften less than R8T in the whole temperature range of 500 to 725°C (Fig. 4.2), most likely due to enhanced high temperature stability by higher levels of silicon and manganese.

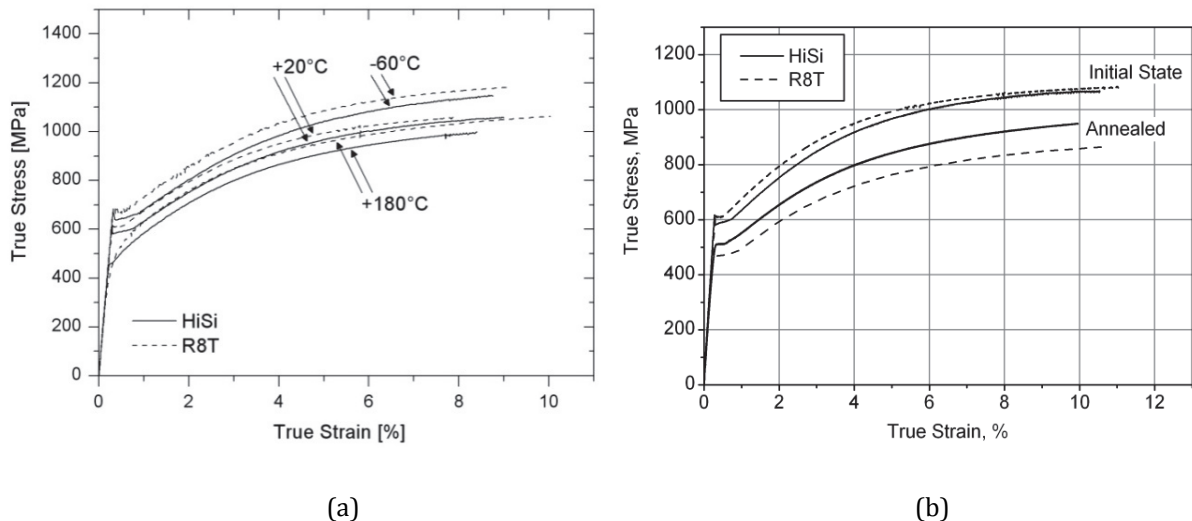


Fig. 4.1: (a) Monotonic stress-strain development as function of temperature. (a) HiSi-R8T materials in initial state at a strain rate of $10^{-4}\cdot s^{-1}$ for three different test temperatures. (b) Annealed material (700°C 28 min) compared to initial state of HiSi-R8T materials at room temperature at a strain rate of $10^{-4}\cdot s^{-1}$.

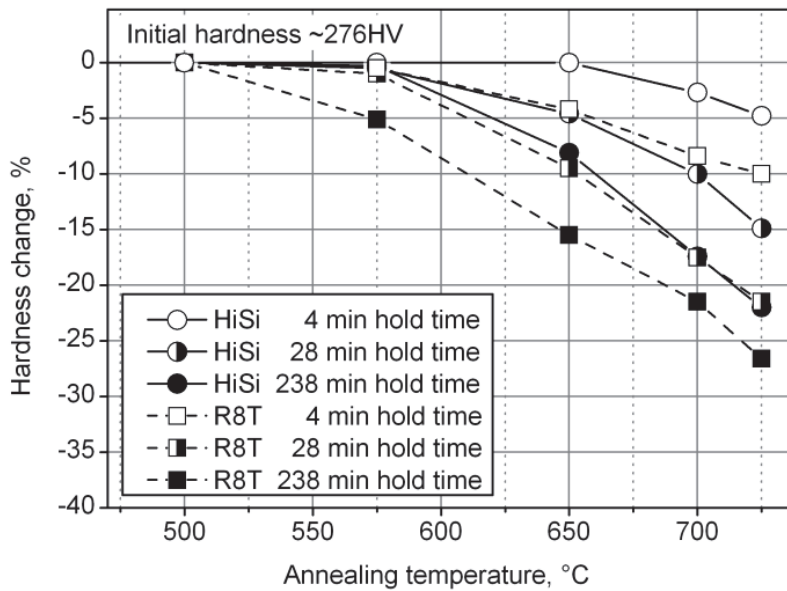


Fig. 4.2: Hardness change as function of annealing temperature and time.

As seen by monotonic testing, initial hardness at room temperature provides a good prediction of cyclic loading behaviour. If the development cyclic stress amplitude is normalized for initial hardness, a similar value of the stress amplitude at $N_f/2$ is obtained for both materials. However, when the materials were annealed prior to testing, HiSi showed a superior LCF behaviour. Thus, the less softened HiSi material had higher stress amplitude until failure. While this difference at first glance did not appear to be significant, as demonstrated with Wöhler plots created from strain controlled measurements in paper II, small changes in stress amplitude may have a significant effect on the component life when the evaluation is done in stress controlled condition, Fig. 5.3. Fig. 4.2

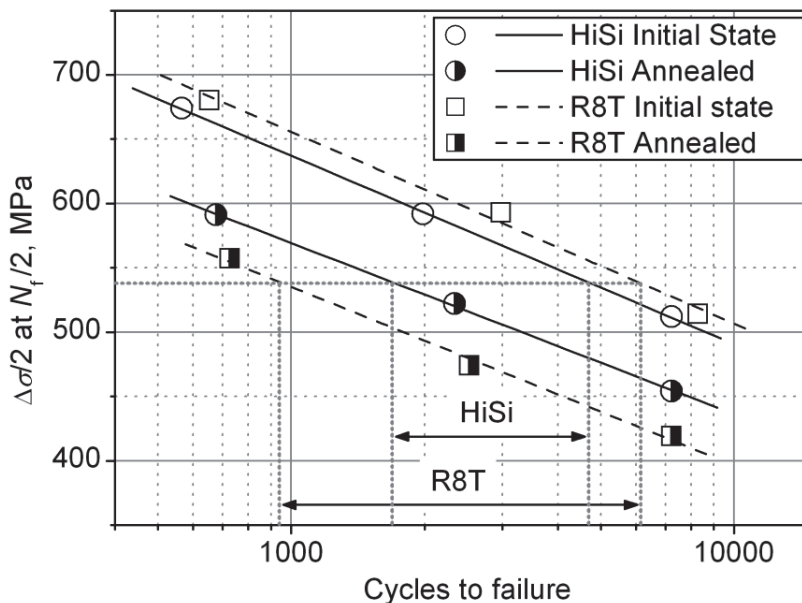


Fig. 4.3: Fitted Wöhler curves demonstrate decrease of fatigue life for two different steel grades caused by annealing (700°C 28 min), analogous for all stress amplitudes.

4.2 Influence of work hardening on annealing softening

Mechanical pre-deformation of material was made in laboratory environment in an attempt to reproduce the heavily deformed surface tread layer. In Paper II it was showed that after subsequent annealing at temperatures comparable to where the virgin material showed none or only small softening, materials exhibited a pronounced softening, and lower effective minimum annealing temperature. Thus, plastic deformation promotes an increased softening rate as could be expected due to processes like recovery and recrystallisation. In paper V similar trials were performed for used wheels where samples were extracted from the tread surface. These highly deformed layers also showed a higher softening rate and lower annealing temperature compared to the virgin deformed material, thus confirming initial laboratory experiment. Although softening could not be measured to take place in the material extracted from the used wheel treads below some 450°C, thermal analysis with DSC indicated that recovery possibly was taking place at lower temperatures. However, rapid annealing trials performed in the range of ca. 1 to 10 seconds in Paper V, showed that the deformed tread layer for these short heating times experienced limited permanent softening at temperatures close to 600°C. Except for the case of a long wheel lockup, the heating duration is expected to be considerably shorter than seconds in the wheel-rail interface under normal running conditions.

4.3 Morphology of pearlite in the tread surface

For used “undamaged wheels”, three characteristic depth regions below the wheel tread surface were distinguished in paper V. In the region closest to the surface, the material is heavily deformed and sheared along the surface, having almost no typical pearlite ferrite microstructural features. Within a transition region the grain size and microstructure morphology is seen to still be affected, but plastic flow gradually decreases with depth. At around 5-10 millimetres below the tread the microstructure becomes homogenous and no plastic flow can be detected. Total depth of deformation naturally varies in-between different wheels and positions in the tread, but the relative sizes of the depth regions are similar.

For the current studied steels, even though the chemical composition was slightly different, the ISP of pearlite and ferrite morphology was seen to govern material properties of virgin wheel material. It was clear that when the alloys were exposed to temperatures above 500°C the softening was due to a partial break up and spheroidisation of lamellar cementite in the pearlite. Pre-deformation performed before annealing, likewise shear deformation in used wheel accelerated the spheroidisation effects leading to a very fine broken down lamella structure. These effects can also be observed in the SEM micrographs from the tread layer in used wheels, shown in Fig. 4.4, where cementite lamellas in the pearlite are close of being globular. Therefore it may be anticipated that the morphology changes in service is due to several combined effects as plastic deformation and thermal loading which will influence the mechanical properties

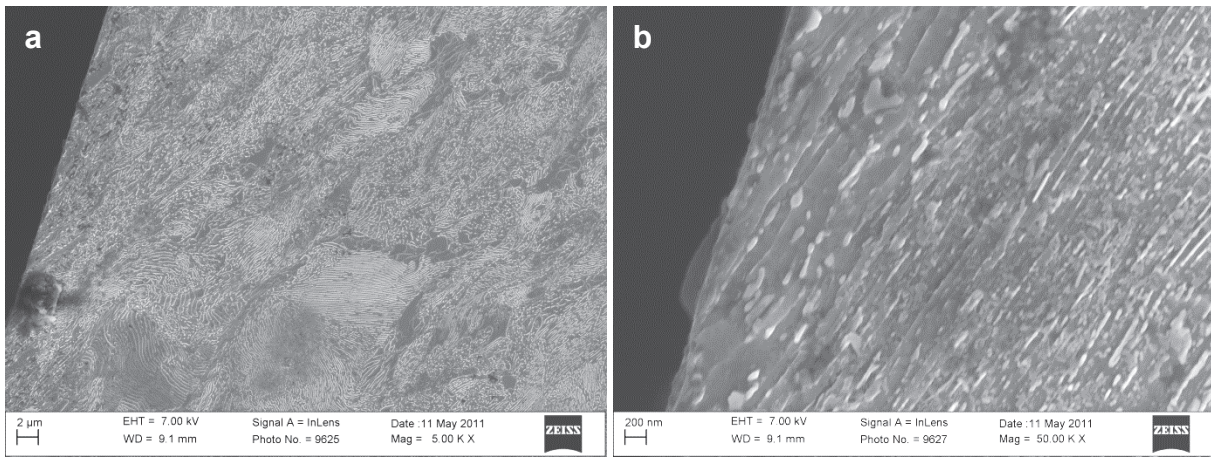


Fig. 4.4: SEM micrographs of cross section in the middle of the wheel tread surface of a used wheel, along the rolling direction (tread surface to the right). (a) Alignment of the microstructure, large plastic shear together with deterioration of the ferrite cementite morphology within pearlite grains can be observed. (b) Most close to the tread surface, the cementite lamella are partially spheroidised

and consequently the response of the material to further loading. From the SEM micrographs (Fig. 4.4), the strong linearization of the microstructure can also be observed in the direction of the shear strain.

Characterisation of anisotropy in the tread as a function of tread position and direction was conducted in paper V. This gave information about which parts of the tread surface undergoes largest deterioration, being more sensitive to damage and how the loading had been in traffic. As shown in Fig. 2.2, the tread surface can be divided in three main characteristic zones. Zone 3, the centre part of the tread is in contact with the rail typically during straight track and zones 1 and 2 are in contact with the rail in curves. Hardness profiling in cross sections in the tread of used wheels presented a significant increased hardness in zones 1 and 2. In the centre zone 3, an increased hardness in the surface compared to virgin wheels was as well measured but the hardness was overall much lower than in zones 1 and 2. This confirms that loading forces during straight track are lower than in curves. Comparing the hardness in the tread surface to the measurements of plastic flow, i.e. shear strain, Fig. 4.5, a good consistency of results were found. In zone 3 significantly less material flow was measured than the outer tread regions. Moreover, shear was not only present in tangential direction but also in transversal direction to the rolling direction. In some regions almost equivalent magnitude of flow stress was measured, giving a total flow component more or less 45° to the rolling direct. It was seen from profiling and sectioning of cracks, that surface RCF cracks closely followed this plastic material flow in both tangential and transversal direction. Hence, these results illustrate that plastic material flow is an important effect to consider. To have accurate predictions and for numerical analysis of crack propagation, these anisotropy effects therefore should be accounted for.

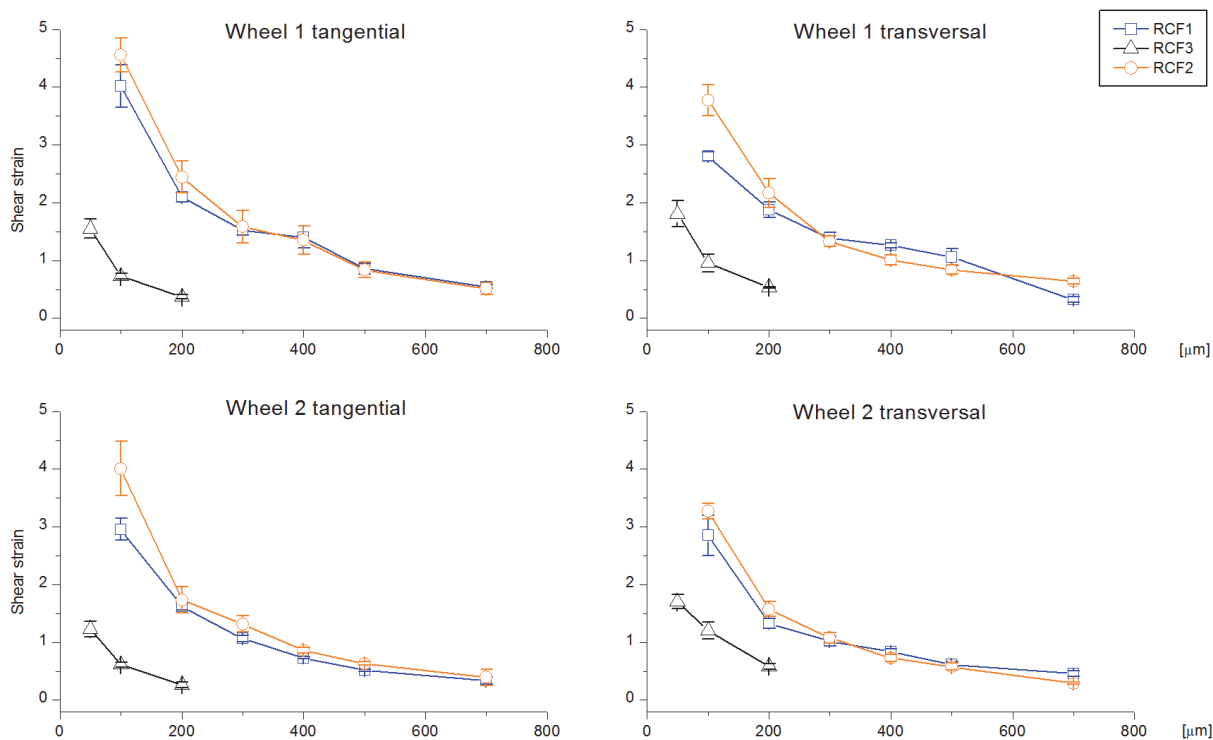


Fig. 4.5: Magnitude of the shear strains in the wheel tread as a function of depth (μm) below the surface measured for tangential and transversal direction in two wheels. Highest shear deformation exist closest to the surface. In the middle of the tread, RCF zone 3, considerable less plastic deformations has been present than in zone 1 and 2.

4.4 Rapid tempering of martensite

As earlier discussed the presence of very large regions of martensite on the tread surface would be an indication of non favourable running conditions. However, due to micro slip it is probably that from time to time smaller regions of martensite still will be formed at the surface. When martensite have just been created at the tread surface, initially compressive stresses are present [9]. When a smaller volume of martensite is tempered, even at rather low temperatures, (below A_1) the residual stress field can change dramatically as shown in paper III. Tensile stresses can be induced since transformation from bct to bcc is accompanied with a substantial volume decrease. The material response was characterised with rapid laser tempering and dilatometry experiments in paper III and IV. It was seen that initially almost no energy barrier exists for the martensite to undergo tempering. For tempering tests performed from several minutes down to 0.1 s, a large decrease in hardness, close to 50% was measured for tempering in the whole time range for temperatures at about 600 to 700°C. The rapid tempering together with the long-time furnace trials showed for the current material that after the initial instant decrease of hardness takes place only little further decrease takes place after several minutes. Therefore, the tempering process depended mainly on the peak temperature. Finite element modelling showed residual stresses being able to develop after local heating in as-quenched martensite solely by the effect of volume decrease, independent of heating rate. For the case of tempered martensite or pearlite, the residual stress field depends both on the heating rate and peak temperature giving

sufficiently large thermal strain gradients to cause local plastic deformation. This results in larger stress gradients, with tensile stress in the surface and compressive below. This is in contrast to as-quenched martensite which exhibits a broad tensile residual stress distribution around the whole tempered volume. These results were qualitatively confirmed with X-ray residual stress measurement of both martensite and pearlite radiated specimens. Rapid tempering trials also were performed under the influence of compressive loading in paper IV for different tempering times and pre-stress levels, see Fig. 4.6. In addition conventional monotonic stress-strain trials were performed for tempered martensitic specimens at elevated temperatures. It was observed that the effective yield stress decreased for martensite when the tempering process was made under external loading. This lower resistance to plastic deformation was believed to be caused by microstrain taking place in the martensite around already high stressed dislocations in the bct crystallographic structure, allowing slip at lower stress when an external load was added [64]. Hence, in wheel-rail contact where thermal loading take place in parallel with mechanical loading, plastic deformation may initiate for lower temperatures than predicted from traditional monotonic stress-strain experiments of tempered material.

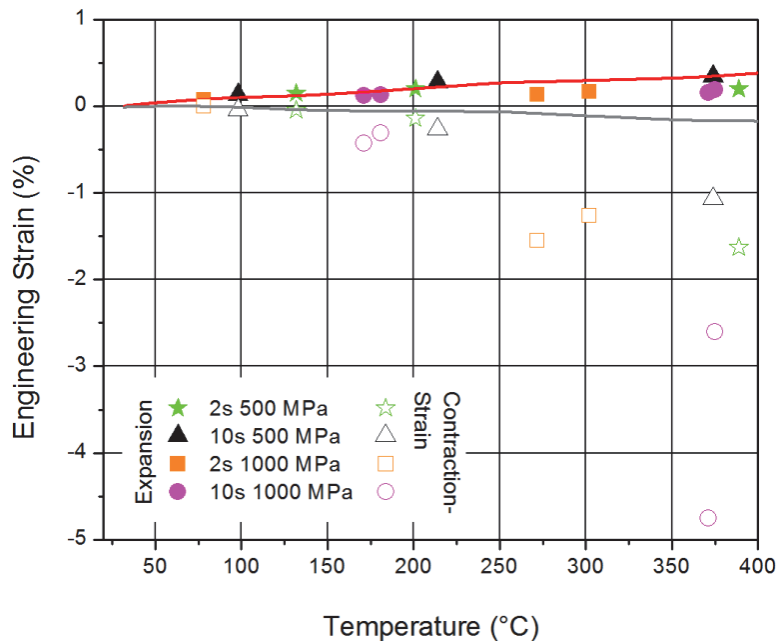


Fig. 4.6: Maximum thermal expansion and shrinkage-plastic strain measured during flash heating for martensitic material in compression. The solid lines represents linear expansion and shrinkage respectively, as measured by dilatometry (no loading). Above ca. 150°C it is seen that pre-loading cause plastic deformation to take progress during tempering.

4.5 Wear residuals within developed rolling contact fatigue cracks

Residuals within cracks in railway wheels, (Fig. 4.7 Fig. 4.7), were studied in paper VI with the aim to investigate chemical composition and how such material could be created. In previous studies of RCF cracks, it has been observed that cracks are not empty, but contains some kind of material, often interpreted to be non-metallic inclusions, martensite, fine-grained deformed material, corrosion products or oxides etc. The investigation made in paper VI showed the material within cracks to mainly consist of sheared out metallic material from the crack faces.

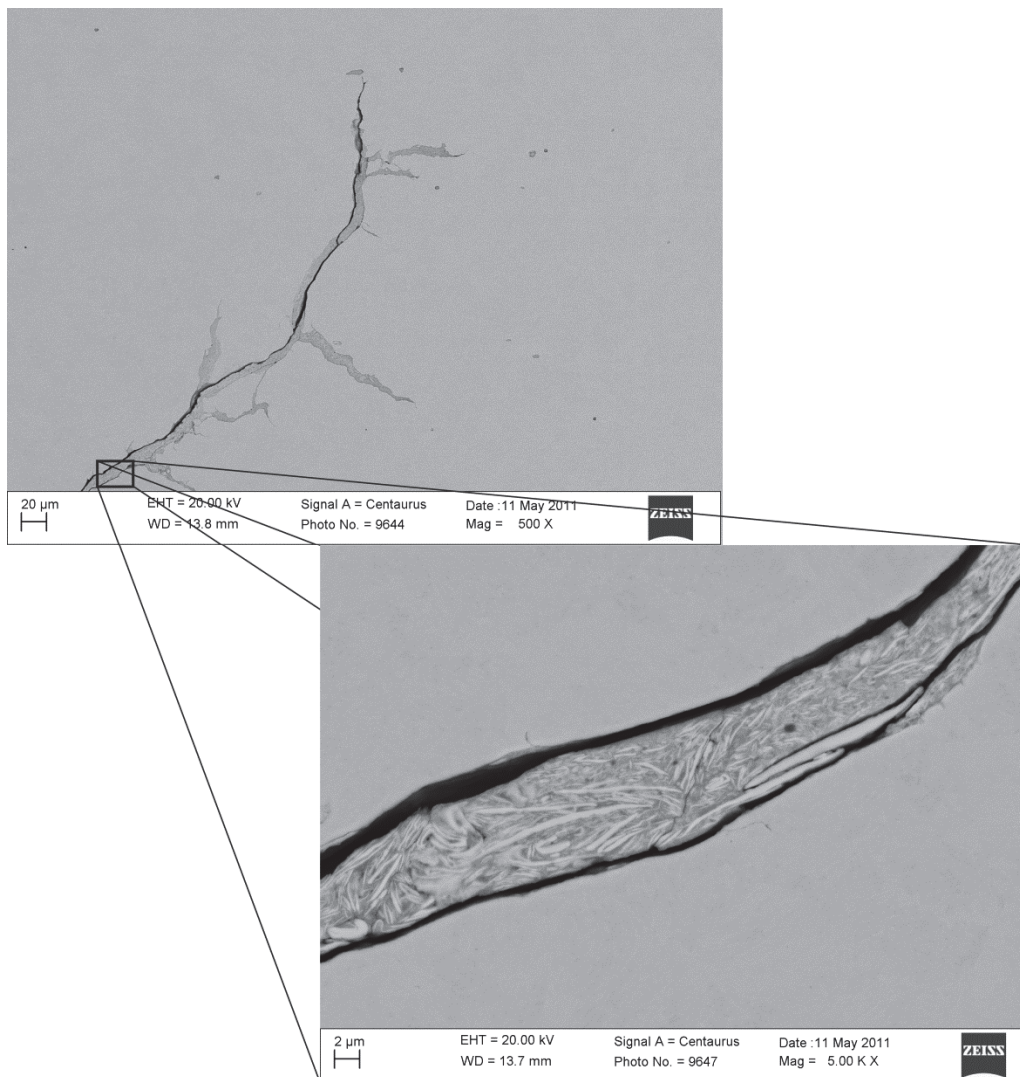


Fig. 4.7: Low magnification SEM (BE) micrograph of subsurface crack branching in the top image. At higher magnification (lower image) the material present within the crack can be seen to consist of mainly metallic flakes and wear debris.

An interesting additional observation was that surface RCF cracks had in some regions a very similar appearance to larger subsurface cracks. The residual crack material, together with plastic deformation and crack branching also provided evidence about possible crack growth mechanisms. Mixed mode crack propagation in compression can

likely be plausible where mode II and III contribute to rubbing and plastic shearing of crack faces. Earlier work by others has shown that crack branching in mixed mode II and III under compressive is possible depending on the crack face frictional force [86-90]. Fluid penetration into already formed cracks in traffic may be a significant factor affecting crack growth, but related mainly to changes in available friction between crack faces [91].

4.6 Concluding remarks and contribution to the field

To study the effects of rapid thermal loading, several different mechanical experiments were performed and microstructures were investigated. It became evident during this process that the complex loading case present in the wheel-rail contact has several implications which make it challenging to study the phenomena in laboratory. For the current topic of interest; rapid thermal heating, one needs to be able to capture the additional effects due to large compressive loads, plastic deformation, wear, material softening, crack propagation, residual stresses etc. which proved to be difficult. While each effect or process may be studied individually, the response from different concurrent process may not always be assumed to be directly additive.

The main conclusions of this investigation are summarised in the following:

- Permanent changes in mechanical properties were not observed in pearlitic material for the typical very short heating times in the wheel-rail contact below austenitisation temperature. Nonetheless, for high temperature mechanical loading, the decrease of the load bearing capability of the material most probably ease plastic deformation and wear, i.e. secondary damage mechanisms, to progress. On the other hand if continuous long term thermal loading is present, as for long time braking or by several consecutive localised heat pulses in the tread surface, thermal loading itself may have a permanent impact on mechanical properties of the material. For this case, the presence of severe plastic deformation and the alloying composition of the material do influence the mechanical material response.
- Pearlitic wheel material was quenched hardened to obtain martensitic structure. At room temperature the martensite has high strength, but the material is sensitivity to tempering at elevated temperatures. Even at moderate temperatures of a few hundred degrees, extensive softening was observed to be taking place for heating pulses of less than a tenth of a second. The softening was even more pronounced when compressive load was added during the tempering process, as typically present in wheel-rail contact.
- Residual stresses, due to local rapid heating can be created even at moderate temperatures. High heating rate is needed for creation of residual stresses in pearlitic material, while for martensite residual stresses can be created already at low temperatures independent of time or heating rate. Due to the tempering behaviour of martensite, with instant softening at rather low temperatures and volumetric

shrinkage, the residual stress field will extend deeper below the surface compared to pearlite for the same heating conditions.

- Within rolling contact fatigue cracks in used wheels, at the surface and deeper below the surface, residual debris was identified, often extending along the whole length of cracks. The analysis of these residuals showed that they predominantly consisted of wear debris and larger metallic fragments. Also, large plastic shear deformation was observed at and adjacent to the crack faces. Thus, this suggests that the cracks have been loaded and propagated in a mixed mode during service, with mode II and III being dominant.

5 Suggestions for further work

There are many ways in which the present work could be continued. Here some topics are presented that would be of interest to investigate in the near future.

- Extended LCF trial matrix that includes a wider temperature range as compared to the present, for better classification of railway steel materials. An alternative is to run LCF at room temperature and flash heat the specimen at ordered intervals to include the effects of thermal loading on the work hardening behaviour. At higher temperatures plastic deformation can progress easier, hence a test method needs to be developed that allows for very high strain in compression to obtain closer reproduction of the actual loading case between wheel and rail.
- The rapid tempering of martensite for the current steel as examined in papers III and IV, particularly under the influence of external applied stresses would be desirable to study further to differentiate the effect of heating time and applied load. A deeper investigation of how the microstructural changes are progressing during this process by SEM or TEM would also be meaningful.
- Attempt to include initial microstructural properties like anisotropy and presence of defects such as short surface RCF cracks, within numerical analysis of thermal stress development in both pearlitic and martensitic material.
- The investigation of rolling contact fatigue cracks in the wheel tread surface as reported in paper VI, suggested that cracks propagate in a mixed mode. Hence, the process of hydrostatic fluid driven cracks in the wheel tread may perhaps not be as central for crack propagation as earlier suggested by other authors. Frictional forces between crack faces and effects from example fluid penetration would therefore be interesting to study further and quantify. A method could be to perform LCF crack propagation trials in compression-torsion within a controlled environment, where humidity and temperature can be varied independently.

Acknowledgements

First of all, I would like to thank and express my gratitude to my supervisor Johan Ahlström for guidance throughout this whole work. His patience is endless and his help have been invaluable. I would further like to thank my two examiners which I had during this work, Professor Birger Karlsson and Professor Christer Persson, for giving me the opportunity to work within this field. I especially appreciate the freedom to follow my ideas and support in pursuing them, both practical and theoretical.

During these years many people in the department have provided help and support with technical and administrative matters, I especially want to recognize: Peter Sotkovsky, Sandra Arvidsson, Göran Fritze, Eduard Hryha, Urban Jelvestam, Håkan Millqvist, Mats Norell, Dick Olofsson, Roger Sagdahl and Yiming Yao.

This project was made within the framework of the Centre of Excellence CHARMEC (Chalmers Railway Mechanics), together with the support of several industrial partners; Bombardier Transportation, Interfleet technology, Lucchini Sweden and Trafikverket. I am gratefully for their financial contribution, in kind contribution of material and all interesting meetings and ideas those have brought forward.

After five years at the department a lot of close friends have been made and some memorable moments I will bring with me forever! Finally, I want to thank Ruth for her support during writing of the thesis, patience, presence during late working days in the lab and always being there when most needed.

References

- [1] A. Ekberg, E. Kabo, Fatigue of railway wheels and rails under rolling contact and thermal loading—an overview, *Wear*, 258 (2005) 1288-1300.
- [2] E. Kabo, A. Ekberg, Material defects in rolling contact fatigue of railway wheels—the influence of defect size, *Wear*, 258 (2005) 1194-1200.
- [3] Wheel-rail interface handbook, First ed., CRC Press, 2009.
- [4] R. Deuce, Wheel tread damage - an elementary guide, Netphen, 2007.
- [5] M.A. Tanvir, Temperature rise due to slip between wheel and rail—an analytical solution for hertzian contact, *Wear*, 61 (1980) 295-308.
- [6] K. Knothe, S. Liebelt, Determination of temperatures for sliding contact with applications for wheel-rail systems, *Wear*, 189 (1995) 91-99.
- [7] F.D. Fischer, E. Werner, W.Y. Yan, Thermal stresses for frictional contact in wheel-rail systems, *Wear*, 211 (1997) 156-163.
- [8] F.D. Fischer, W. Daves, E.A. Werner, On the temperature in the wheel-rail rolling contact*, *Fatigue & Fracture of Engineering Materials & Structures*, 26 (2003) 999-1006.
- [9] J. Ahlström, B. Karlsson, Microstructural evaluation and interpretation of the mechanically and thermally affected zone under railway wheel flats, *Wear*, 232 (1999) 1-14.
- [10] D.T. Llewellyn, Steels metallurgy & applications, 2nd ed., Butterworth-Heinemann Ltd, Oxford, 1995.
- [11] K. Cvetkovski, J. Ahlström, B. Karlsson, Thermal softening of fine pearlitic steel and its effect on the fatigue behaviour, (2010).
- [12] K. Cvetkovski, J. Ahlström, B. Karlsson, Monotonic and Cyclic Deformation of a High Silicon Pearlitic Wheel Steel, *Wear*, 271 (2011) 382-387.
- [13] R. Song, D. Ponge, D. Raabe, R. Kaspar, Microstructure and crystallographic texture of an ultrafine grained C-Mn steel and their evolution during warm deformation and annealing, *Acta Mater.*, 53 (2005) 845-858.
- [14] F. Wetscher, R. Stock, R. Pippan, Changes in the mechanical properties of a pearlitic steel due to large shear deformation, *Mater. Sci. Eng., A*, 445-446 (2007) 237-243.
- [15] D.I. Fletcher, Thermal contact stress and near surface rail cracks, 9th International Conference on Contact Mechanics and Wear of Rail/Wheel Systems, Chengdu, China, 2012, pp. 470-479.
- [16] M. Clarke, Wheel rolling contact fatigue (RCF) and rim defects investigation to further knowledge of the causes of RCF and to determine control measures, *Wheel Steels Handbook*, 2008.
- [17] P.J. Mutton, C.J. Epp, J. Dudek, Rolling contact fatigue in railway wheels under high axle loads, *Wear*, 144 (1991) 139-152.
- [18] J. Kalousek, M. Magel, Achieving a balance : The "magic" wear rate, *Railway Track & Structures (RT & S)*, 3 (1997).

- [19] E. Lansler, E. Kabo, Subsurface crack face displacements in railway wheels, *Wear*, 258 (2005) 1038-1047.
- [20] P.T. Torstensson, Rail Corrugation Growth on Curves, Department of Applied Mechanics, Chalmers University of Technology, 2009.
- [21] A.F. Bower, K.L. Johnson, Plastic flow and shakedown of the rail surface in repeated wheel-rail contact, *Wear*, 144 (1991) 1-18.
- [22] J. Tunna, J. Sinclair, J. Perez, A review of wheel wear and rolling contact fatigue, *Proc. Inst. Mech. Eng. Part F J. Rail Rapid Transit*, 221 (2007) 271-289.
- [23] R. Enblom, Deterioration mechanisms in the wheel-rail interface with focus on wear prediction: A literature review, *Veh. Syst. Dyn.*, 47 (2009) 661-700.
- [24] H. Hertz, Über die Berührung fester elastischer Körper, *Journal für reine und angewandte Mathematik*, 92 (1882) 156-171.
- [25] S. Suresh, *Fatigue of materials*, Second ed., University Press, Cambridge, 2004.
- [26] A. Pieringer, Modelling of wheel/rail interaction considering roughness and discrete irregularities, Institutionen för bygg- och miljöteknik, Teknisk akustik, Vibroakustik, Chalmers tekniska högskola, 2008, pp. 70+12+76.
- [27] A. Kapoor, F.J. Franklin, S.K. Wong, M. Ishida, Surface roughness and plastic flow in rail wheel contact, *Wear*, 253 (2002) 257-264.
- [28] Spårtrafiksystem och spårfordon, 4th ed., Stockholm, 2007.
- [29] K. Cvetkovski, J. Ahlström, Characterisation of plastic deformation and thermal softening of the surface layer of railway passenger wheel treads, Submitted to *Wear*, (2012).
- [30] A. Ekberg, E. Kabo, Fatigue of railway wheels and rails under rolling contact and thermal loading-an overview, *Wear*, 258 (2005) 1288-1300.
- [31] K.L. Johnson, A shakedown limit in rolling contact, 4th Natl. Conf. on Applied Mechanics, Berkeley, California, 1962, pp. 971-975.
- [32] A. Satyadevi, S.M. Sivakumar, S.S. Bhattacharya, A new failure criterion for materials exhibiting ratcheting during very low cycle fatigue, *Materials Science and Engineering: A*, 452-453 (2007) 380-385.
- [33] N.E. Dowling, *Mechanical behaviour of material: engineering methods for deformation, fracture, and fatigue*, Second ed., Prentice-Hall, New Jersey, 1999.
- [34] T.R. Vantiger, R.I. Stephens, M. Karadag, The influence of high R ratio on notched fatigue behaviour of 1045 steel with three different heat treatments, *Int. J. Fatigue*, 24 (2002) 1275-1284.
- [35] P. Clayton, Tribological aspects of wheel-rail contact: a review of recent experimental research, *Wear*, 191 (1996) 170-183.
- [36] C. Jones, W. Tyfour, J. Beynon, A. Kapoor, The effect of strain hardening on shakedown limits of a pearlitic rail steel, *Proc. Inst. Mech. Eng. Part F J. Rail Rapid Transit*, 211 (1997) 131-140.

- [37] A. BÖHMER, M. ERTZ, K. KNOTHE, Shakedown limit of rail surfaces including material hardening and thermal stresses, *Fatigue & Fracture of Engineering Materials & Structures*, 26 (2003) 985-998.
- [38] A. Kapoor, K.L. Johnson, Effect of changes in contact geometry on shakedown of surfaces in rolling/sliding contact, *Int. J. Mech. Sci.*, 34 (1992) 223-239.
- [39] K. Handa, Y. Kimura, Y. Mishima, Ferrite and Spheroidized Cementite Ultrafine Microstructure Formation in an Fe-0.67 Pct C Steel for Railway Wheels under Simulated Service Conditions, *Metall. Mater. Trans. A*, 40 (2009) 2901-2908.
- [40] K.M. Lee, A.A. Polycarpou, Wear of conventional pearlitic and improved bainitic rail steels, *Wear*, 259 (2005) 391-399.
- [41] H.A. Aglan, Z.Y. Liu, M.F. Hassan, M. Fateh, Mechanical and fracture behavior of bainitic rail steel, *J. Mater. Process. Technol.*, 151 (2004) 268-274.
- [42] O.P. Modi, N. Deshmukh, D.P. Mondal, A.K. Jha, A.H. Yegneswaran, H.K. Khaira, Effect of interlamellar spacing on the mechanical properties of 0.65% C steel, *Mater. Charact.*, 46 (2001) 347-352.
- [43] T. Gladman, I.D. McIvor, F.B. Pickering, SOME ASPECTS OF THE STRUCTURE-PROPERTY RELATIONSHIPS IN HIGH-CARBON FERRITE-PEARLITE STEELS, *J Iron Steel Inst (London)*, 210 (1972) 916-930.
- [44] J. Hyzak, I. Bernstein, The role of microstructure on the strength and toughness of fully pearlitic steels, *Metall. Mater. Trans. A*, 7 (1976) 1217-1224.
- [45] A. Marder, B. Bramfitt, The effect of morphology on the strength of pearlite, *Metall. Mater. Trans. A*, 7 (1976) 365-372.
- [46] R.W.K. Honeycombe, H.K.D.H. Bhadeshia, *Steels microstructure and properties*, 2nd ed., Butterworth-Heinemann, Oxford, 2000.
- [47] U. Singh, A. Popli, D. Jain, B. Roy, S. Jha, Influence of microalloying on mechanical and metallurgical properties of wear resistant coach and wagon wheel steel, *J. Mater. Eng. Perform.*, 12 (2003) 573-580.
- [48] Z.Q. Lv, S.H. Sun, Z.H. Wang, M.G. Qv, P. Jiang, W.T. Fu, Effect of alloying elements addition on coarsening behavior of pearlitic cementite particles after severe cold rolling and annealing, *Mater. Sci. Eng., A*, 489 (2008) 107-112.
- [49] B.L. Bramfitt, A.O. Benscoter, *Metallographer's Guide: Irons and Steels*, ASM International, Materials Park, OH 44073-0002, 2002.
- [50] K. Cvetkovski, J. Ahlström, M. Norell, S. Persson, Analysis of wear debris in rolling contact fatigue of pearlitic railways wheels, Submitted to *Wear*, (2012).
- [51] H. F.J., H. M., *Recrystallization and related annealing phenomena*, Second Edition ed., Elsevir Oxford, 2004.
- [52] K. Handa, Y. Kimura, Y. Yasumoto, T. Kamioka, Y. Mishima, Effect of deformation and annealing temperatures on ultrafine microstructure development and yield strength of pearlitic steel through continuous recrystallization, *Mater. Sci. Eng., A*, 527 (2010) 1926-1932.
- [53] R. Abbaschian, L. Abbaschian, R.E. Reed-Hill, *Physical Metallurgy Principles*, Fourth Edition ed., Cengage Learning, Stamford, 2010.

- [54] R.W. Cahn, Chapter 28 - Recovery and Recrystallization, in: W.C. Robert, H. Peter (Eds.) *Physical Metallurgy (Fourth Edition)*, North-Holland, Oxford, 1996, pp. 2399-2500.
- [55] Chapter 5 Softening mechanisms, in: J.D.I.S. Bert Verlinden, D.D. Roger (Eds.) *Pergamon Materials Series*, Pergamon, 2007, pp. 83-108.
- [56] T. Tarui, T. Takahashi, S. Ohashi, R. Uemori, Effect of silicon on the age softening of high carbon steel wire, *I & SM*, 21 (1994) 25-30.
- [57] G. Miyamoto, J.C. Oh, K. Hono, T. Furuhashi, T. Maki, Effect of partitioning of Mn and Si on the growth kinetics of cementite in tempered Fe-0.6 mass% C martensite, *Acta Mater.*, 55 (2007) 5027-5038.
- [58] E. Kozeschnik, H.K.D.H. Bhadeshia, Influence of silicon on cementite precipitation in steels, *Mater. Sci. Technol.*, 24 (2008) 343-347.
- [59] Chapter 7 Phase transformations, in: J.D.I.S. Bert Verlinden, D.D. Roger (Eds.) *Pergamon Materials Series*, Pergamon, 2007, pp. 127-150.
- [60] H.K.D.H. Bhadeshia, R. Honeycombe, *Steels: Microstructure and Properties*, Third Edition, Elsevier Ltd., 2006.
- [61] H.K.D.H. Bhadeshia, S.R. Honeycombe, 9 - The Tempering of Martensite, *Steels (Third Edition)*, Butterworth-Heinemann, Oxford, 2006, pp. 183-208.
- [62] D.A. Porter, K.E. Easterling, *Phase transformations in metals and alloys*, Second edition ed., Stanley Thornes Ltd, Cheltenham, 2001.
- [63] G.R. Speich, W.C. Leslie, TEMPERING OF STEEL, *Metall Trans*, 3 (1972) 1043-1054.
- [64] G. Krauss, Martensite in steel: strength and structure, *Materials Science and Engineering: A*, 273-275 (1999) 40-57.
- [65] R.C. Sharma, *Principles of Heat Treatment of Steels*, First edition ed., New age international limited, publishers, Delhi, 2008.
- [66] J. Pacyna, Dilatometric investigations of phase transformations at heating and cooling of hardened, unalloyed, high-carbon steels, *Journal of Achievements in Materials and Manufacturing Engineering*, 46 (2011).
- [67] K. Cvetkovski, J. Ahlström, B. Karlsson, Influence of short heat pulses on properties of martensite in medium carbon steels, Submitted to *Materials Science and Engineering A*, (2012).
- [68] M. Umemoto, X. Hao, T. Yasuda, K. Tsuchiya, Formation and annealing behavior of nanocrystalline steels produced by ball drop test, *Materials Transactions*, 43 (2002) 2536-2542.
- [69] K. Rytberg, M. Knutson Wedel, P. Dahlman, L. Nyborg, Microstructural evolution during fracture induced by high strain rate deformation of 100Cr6 steel, *J. Mater. Process. Technol.*, 209 (2009) 3325-3334.
- [70] N. Ridley, A Review of the Data on the Interlamellar Spacing of Pearlite, *Metall. Mater. Trans. A*, 15 (1984) 1019-1036.
- [71] ASTM E 92: Standard Test Method for Vickers Hardness of Metallic Materials, American Society for Testing and Materials, Philadelphia, 1990.

- [72] ASTM E 348: Standard Test Method for Microhardness of Materials, American Society for Testing and Materials, Philadelphia, 1990.
- [73] P.S. Prevey, X-Ray Diffraction Residual Stress Techniques, ASM Metals Handbook, 1986, pp. 380-392.
- [74] Lambda Technologies, Determination of Volume Percent Retained Austenite by X-Ray Diffraction, Diffraction Notes, 5521 Fair Lane, Cincinnati, OH 45227, 2006.
- [75] D. Aliya, S. Lampman, Physical Metallurgy Concepts in Interpretation of Microstructures ASM Metals Handbook, 2004, pp. 44-70.
- [76] R.F. Speyer, Thermal Analysis of Materials, Marcel Dekker, INC, New York, 1994.
- [77] ASM Ready Reference: Thermal Properties of Metals (Materials Data Series), ASM International, Materials Park, OH 44073-0002, 2002.
- [78] G. Van der Plaats, The Practice of Thermal Analysis, Mettler, Switzerland.
- [79] F. Scholz, E. Woldt, The Release of Stored Energy during Recovery and Recrystallization of Cold Rolled Ultra High Purity Iron, J. Therm. Anal. Calorim., 64 (2001) 895-903.
- [80] F. Scholz, J.H. Driver, E. Woldt, The stored energy of cold rolled ultra high purity iron, Scr. Mater., 40 (1999) 949-954.
- [81] J.F. Watts, J. Wolstenholme, An Introduction to Surface Analysis by XPS and AES, 2nd Edition ed., Wiley-Blackwell, 2003.
- [82] P.R.N. Childs, Practical Temperature Measurement, Butterworth-Heinemann, Oxford, 2001.
- [83] R.E. Bentley, Handbook of temperature measurement, Theory and practice of thermoelectric thermometry, Springer, cop, Singapore 1998.
- [84] Pyrometer-Handbook, in: I.I. GmbH (Ed.) Non-Contact Thermometry, IMPAC Infrared GmbH, Frankfurt am Main, Germany, 2004.
- [85] Handbook of Infra-red Detection Technologies Elsevier Advance Technology, Oxford, UK, 2002.
- [86] L.M. Keer, M.D. Bryant, A Pitting Model for Rolling Contact Fatigue, J. Lubr. Technol., 105 (1983) 198-205.
- [87] A. Otsuka, K. Mori, T. Miyata, The condition of fatigue crack growth in mixed mode condition, Eng. Fract. Mech., 7 (1975) 429-439.
- [88] H. Matsunaga, N. Shomura, S. Muramoto, M. Endo, Shear mode threshold for a small fatigue crack in a bearing steel Fatigue & Fracture of Engineering Materials & Structures, 34 (2011) 72-82.
- [89] S. Beretta, S. Foletti, K. Valiullin, Fatigue strength for small shallow defects/cracks in torsion, Int. J. Fatigue, 33 (2011) 287-299.
- [90] M.G. Tarantino, S. Beretta, S. Foletti, J. Lai, A comparison of Mode III threshold under simple shear and RCF conditions, Eng. Fract. Mech., 78 (2011) 1742-1755.
- [91] A.F. Bower, Influence of crack face friction and trapped fluid on surface initiated rolling contact fatigue cracks, 1988.

